

An assessment of transport timescales and return coefficient in adjacent tropical estuaries

Andutta, Fernando P.; Helfer, Fernanda; de Miranda, Luiz Bruner; Deleersnijder, Eric; Thomas, Christopher; Lemckert, Charles

DOI

[10.1016/j.csr.2016.05.006](https://doi.org/10.1016/j.csr.2016.05.006)

Publication date

2016

Document Version

Accepted author manuscript

Published in

Continental Shelf Research

Citation (APA)

Andutta, F. P., Helfer, F., de Miranda, L. B., Deleersnijder, E., Thomas, C., & Lemckert, C. (2016). An assessment of transport timescales and return coefficient in adjacent tropical estuaries. *Continental Shelf Research*, 124, 49-62. <https://doi.org/10.1016/j.csr.2016.05.006>

Important note

To cite this publication, please use the final published version (if applicable).
Please check the document version above.

Copyright

Other than for strictly personal use, it is not permitted to download, forward or distribute the text or part of it, without the consent of the author(s) and/or copyright holder(s), unless the work is under an open content license such as Creative Commons.

Takedown policy

Please contact us and provide details if you believe this document breaches copyrights.
We will remove access to the work immediately and investigate your claim.

An assessment of transport timescales and return coefficient in adjacent tropical estuaries

FERNANDO P. ANDUTTA^{a,b*}, FERNANDA HELFER^a, LUIZ BRUNER DE MIRANDA^b, ERIC

DELEERSNIJDER^{c,d}, CHRISTOPHER THOMAS^e, CHARLES LEMCKERT^a

^a Griffith School of Engineering, Griffith University, Gold Coast, QLD 4222, Australia.

^b Oceanographic Institute, University of São Paulo, São Paulo SP, Brazil, CEP 05508-900, Brazil.

^c Université catholique de Louvain (UCL), Institute of Mechanics, Materials and Civil Engineering (IMMC) & Earth and Life Institute (ELI), 4 Avenue Georges Lemaître, Bte L4.05.02, B-1348 Louvain-la-Neuve, Belgium

^d Delft University of Technology, Delft Institute of Applied Mathematics (DIAM), Mekelweg 4, 2628CD Delft, The Netherlands

^e Université catholique de Louvain (UCL), Institute of Mechanics, Materials and Civil Engineering (IMMC), 4 Avenue Georges Lemaître, Bte L4.05.02, B-1348 Louvain-la-Neuve, Belgium.

Abstract –

Transport timescales (TTS), namely residence time and exposure time, were computed for adjacent shallow meso-tidal tropical estuarines system using the Lagrangian model D-Waq Part coupled with the hydrodynamic model Delft3D-Flow, and the Constituent-oriented Age and Residence time Theory, CART. The main results are threefold: (a) The TTS differs more between releases at high or low tide than between those at spring and neap tides. The exposure time was also calculated and found to be larger than the residence time by a few days. (b) The exposure and residence times were used to evaluate the return coefficient (r) for different scenarios. As with residence and exposure times, the return coefficient was found to differ more between releases at high or low tide than between those at spring and neap tides. (c) For the Caravelas Estuary, where the river inflow was low ($\sim 4 \text{ m}^3 \text{ s}^{-1}$), the residence time was found to be much larger than for the Peruípe Estuary, where the river discharge was greater and nearly constant during the sampling period ($\sim 20 \text{ m}^3 \text{ s}^{-1}$). These results shows the importance of advection in decreasing TTS in the Peruípe Estuary compared to the Caravelas Estuary. The influence of the advection and dispersion agrees with previous simple estimates obtained using the newly modified Land Ocean Interaction Coastal Zone (LOICZ) model by Andutta et al. (2014).

32 Keywords: tropical estuary; residence time; exposure time; return coefficient; numerical model;
33 hydrodynamics.

34

35 **1. Introduction**

36 Since the dynamics of most estuarine systems is relatively complex, studies of transport
37 timescales (TTS) provide valuable insight into estuarine behaviour. Transport timescales represent a
38 more holistic way of interpreting the flow in complex systems (e.g. Monsen et al. 2002), and allow
39 us to understand how advective and dispersive mechanisms transport water.

40 Transport timescales are driven by the water currents, which in turn are influenced by sea
41 level oscillation, bathymetry and the temperature and salinity fields. It is therefore necessary to have
42 an accurate representation of these quantities in order to satisfactorily estimate transport timescales.

43 This article has the following tasks:

44 (1) to demonstrate, using a 3D hydrodynamic model combined with particle simulations,
45 how release times (e.g. slack waters of high and low tides, neap and spring tides) affect the
46 exposure time and residence time in a shallow meso-tidal tropical estuary.

47 (2) to compare TTS results from numerical modelling with estimates using the simple
48 newly modified Land Ocean Interaction Coastal Zone (LOICZ) model by Andutta et al. (2014).

49 (3) to calculate and evaluate the return coefficient (r) numerically and analytically using
50 CART. This is a measure of the propensity of a water parcel to return into the domain of interest
51 after leaving it.

52

53 *a. Overview of Transport Timescales*

54 Since the pioneering work by Ketchum (1951) and Bolin and Rodhe (1973), the theory of
55 TTS has evolved (e.g. CART, www.climate.be/cart), and other TTS definitions have been
56 introduced in order to fill scientific gaps. Therefore, there are many different transport timescale
57 definitions, e.g. flushing time (Ketchum, 1951; Fischer et al., 1979; Monsen et al., 2002), residence

58 time (Bolin and Rodhe, 1973; Monsen et al., 2002; Delhez et al. 2004; Deleersnijder et al., 2006),
 59 exposure time (Monsen et al., 2002), transit time (Holzer and Hall 2000), influence time (Delhez et
 60 al., 2014), age (Bolin and Rodhe, 1973; Monsen et al., 2002), e-folding flushing time (Monsen et
 61 al., 2002), turnover time (Sheldon and Alber, 2006) and renewal time (Andutta et al., 2014) – all of
 62 which have their own interpretation.

63 Two timescales, residence time and exposure time, are used to provide an indication of
 64 increase or decrease of non-reactive and reactive substances in estuaries, bays, lagoons, and atolls
 65 (Andutta et al., 2014). The residence time (Θ) is the time needed for a particle constituent to reach
 66 for the first time an open boundary of the domain of interest (e.g. Delhez et al., 2004). The exposure
 67 time (φ) is the time the particle will stay in the domain (e.g. Monsen et al., 2002) (Figure 2).
 68 Therefore, at a given time and location, the exposure time is always larger than or equal to the
 69 residence time. The larger the difference between the two timescales, the more often the particles
 70 tend to re-enter the domain of interest after leaving it for the first time. To evaluate the exposure
 71 time, the computational domain must be larger than the domain of interest (de Brauwere et al.,
 72 2011, de Brye et al., 2012). Estimates of these timescales may be obtained in an Eulerian or a
 73 Lagrangian framework. The latter often requires sufficiently large number of numerical particles in
 74 order to provide a result that statistically approaches the real condition.

75 A dimensionless return coefficient, r , represents the propensity of particles to return into the
 76 estuary after reaching an open boundary for the first time, as illustrated in Figure 1A (de Brauwere
 77 et al., 2011). It is defined as the relative difference between φ and Θ , i.e.

$$78 \quad r = \frac{(\Theta - \varphi)}{\Theta} . \quad (1)$$

79 Clearly, this coefficient lies in the interval [0,1].

80 The larger the r the more likely it is that particles will re-enter the estuary after crossing one
 81 of its open boundaries for the first time. Accordingly, particles that never return into the estuary
 82 have $r = 0$, while particles returning often or for long periods of time have r close to unity.

83
84
85
86

Preferred position for figure 1

87 *b. Chosen estuary and coastal area*

88 The domain of interest is the estuarine System of the Caravelas and Peruípe Rivers (ESCP),
89 in southern Bahia state, Brazil (see Figure 2); more details may be found in Appendix 1. It is
90 located at the approximate latitude of 17°50'S, nearly 60 km from the National Maritime Park of
91 Abrolhos, which is one of the largest reef structures of the Atlantic ocean, providing habitat for
92 innumerable marine species. The ESCP has two main mouths: the Caravelas Estuary in the north
93 (17°45'S), with two small channels named Barra Velha (~1 km wide) and Tomba's Mouth (~600 m
94 wide), and the Peruípe Estuary in the south (17°54'S) with a funnel shape ranging in width from
95 ~3500 m to ~700 m in the first few hundred meters. These two mouths are separated by a distance
96 of ~25 km alongshore, and are internally connected by shallow and narrow channels around
97 Cassurubá or Cassumba Island. Our simulations consider the domain shown in Figure 1C, for which
98 results were computed according to the number of particles in the control domain with boundaries
99 ω_1 and ω_2 .

100

101

102

103

Preferred position for figure 2

104 **2. Methods**

105

106 *a. Numerical model*

107 The ESCP comprises a number of channels varying significantly in width, from 60 m
108 upstream to 1000 m near the mouth, and thus a high resolution mesh is necessary to resolve the
109 many small channels in the domain. The numerical model used is the curvilinear-mesh, three-
110 dimensional Delft3D-Flow from Deltares (www.deltares.nl). This model is hydrostatic, and its

111 equations are solved by the method of finite differences (Delft Hydraulics, 2008). A curvilinear
112 mesh is appropriate for the domain, although there are some disadvantages in the horizontal
113 resolution distribution compared to unstructured meshes. Delft3D's curvilinear mesh is efficient in
114 minimizing noise due to the steps in the horizontal plane, and allows the mesh cells to follow the
115 channels more easily compared to non-curvilinear quadrangular meshes. The degree of non-
116 orthogonality between mesh elements is always smaller than 0.02 thus satisfying the criteria ($\cos \theta$
117 < 0.02), which helps to preserve numerical stability of the simulations (Delft Hydraulics, 2008).
118 The diagonal horizontal resolution ranges from ~20 m to ~300 m. The number of quadrangular
119 mesh cells on the horizontal plane is 22,928. A lower resolution is applied in the coastal region
120 ~[130-300] m, but this is increased toward the coast and the estuary ~[20-100] m (Figure 1B). The
121 refined mesh within the estuary combined with high water speeds requires the time-step to be
122 relatively small (around 1 second), to satisfy the Courant–Friedrichs–Lewy condition. The mesh
123 used in the simulations of the ESCP (Figure 1B) is relatively complex, covering a small part of the
124 Peruípe River, near the city of Nova Viçosa. This river is the main channel connecting the northern
125 and southern mouths. The main tributaries of the Caravelas River, namely the Cupído and Jaburuna
126 Rivers, are covered by the mesh. With 10 equally spaced sigma vertical layers, this mesh also
127 covers a few kilometers of the adjacent coastal region.

128 The bathymetry in the estuarine channels was obtained using an Echo sounder and Global
129 Position System. Two tide gauges were installed in Caravelas and Nova Viçosa (see locations A and
130 C in Figure 2), meant to remove the tides from the Echo sounder data. For the Peruípe River
131 estuary, the bathymetry was measured only in the first 6 km, near anchor station D. Thus an
132 extrapolation was applied, considering the depth to be 4 meters for the next 14 km along the Peruípe
133 River. The bathymetry was combined from these sources, and the triangular interpolation
134 application in Delft3D-Flow was used. The bottom topography has depths ranging from ~0.2 m to a
135 maximum of ~18 m (Tombo's Mouth), whilst in the coastal region do not exceed ~10 m.

136 A more detailed description of the field work carried out to obtain measurements of
 137 thermohaline properties and other parameters is provided in Appendix 2.

138
 139 *b. Model Boundary conditions, initial conditions and physical parameters*

140 Rainfall and river discharge measurements in the Peruípe River are shown in Figure 3B. The
 141 river discharge data, obtained from the National Agency of Waters ANA (<http://www.ana.gov.br/>),
 142 was measured at a gauge station upstream of the river, at station Helvécia n° 55510000 (code
 143 1739006). This station covers a large part of the drainage basin of the river. During rainy conditions
 144 the total drainage basin of the river may be used to estimate the total river flow to be applied at the
 145 upstream inflow boundary of the river. The factor to account for the missing drainage basin area is
 146 $\alpha = \frac{A_1 + A_2}{A_1} = 1.6$, in which station Helvécia $A_1 \sim 2,840 \text{ km}^2$, and the downstream area not covered
 147 by this gauge station is $A_2 \approx 1,760 \text{ km}^2$. The area values were obtained from the ANA
 148 (<http://hidroweb.ana.gov.br/>).

149 Data from the gauge station were also used to estimate the river discharge range for the
 150 Cupído and Jaburuna rivers. This was done by comparing their watershed areas with the watershed
 151 of the Peruípe river, and assuming homogeneous rainfall and evapotranspiration distributions over
 152 these areas (Andutta, 2011; Pereira et al., 2010). The total river flow into Caravelas Estuary was
 153 then roughly estimated using $Q = Q_P \beta$, where $\beta = 600/4600$ is the ratio between the catchment
 154 areas of the Caravelas (600 km^2) and the Peruípe ($A_1 + A_2 = 4600 \text{ km}^2$) rivers, and Q_P is the
 155 average discharge for the Peruípe). This estimation was adjusted by comparing observed flow
 156 velocities at locations A and B with model predictions.

157 The monthly estimate of fresh water inflow for the Peruípe River reveals small inflow for
 158 the dry season, often between June and September (see Figure 3C). The combined freshwater input
 159 from the Jaburuna and Cupído rivers estimated using the factor β is less than 10% of the river
 160 discharge into the Peruípe River. Because the field work was conducted during a relatively dry wet

161 season, when rainfall was negligible prior to and during measurements obtained in January 2008
162 (Figure 3A), it is logical not to consider the application of the factor α at the Helvécia gauge
163 station. Although this approach of river flow estimation is not required, the technique described
164 above would be required under homogeneous rainfall conditions over the drainage basin of the
165 Peruípe, Jaburuna and Cupído rivers.

166 The best fit between observations and model results was obtained using the mean river
167 discharge shown in Table 1 for the Cupído and Jaburuna rivers, and the daily measurements shown
168 in Figure 3B for the Peruípe River. In other words, the value measured at Helvécia gauge station
169 was used in the simulation with additional tuning to extrapolate results for the other two smaller
170 rivers.

171 .
172 **Preferred position for figure 3**
173
174

175
176 **Preferred position for Table 1**
177

178 The measurements from this tide gauge were compared with the simulation results during
179 neap and spring tides using the “Skill” method described below. In addition, a qualitative
180 comparison was carried out between the axial salinity distribution found in the simulations, and the
181 observed distribution presented in Schettini and Miranda (2010).

182 We used the initial condition of a homogeneous thermohaline distribution for the salinity (30
183 practical salinity unit - psu) and temperature (27 °C). The spin up simulation was made for about
184 two months to obtain a dynamic equilibrium condition. Since the temperature has previously been
185 found to be nearly homogeneous in this estuary (Andutta, 2011), its mean value was used for all
186 simulations. The first flow field and salinity distribution, obtained from the equilibrium condition,

187 was used to provide a varied initial field for simulations starting at slack waters in both spring and
 188 neap tidal conditions.

189 Computational modellers often assume that vertical eddy diffusion and viscosity coefficients
 190 vary in time, by using turbulent closure models, e.g. algebraic, *k-L*, *k-Epsilon* schemes. On the other
 191 hand, the horizontal eddy diffusivity, K_h , and horizontal viscosity coefficients, K_v , are often
 192 estimated according to the mesh element size (Okubo, 1971). Therefore, modellers need to choose a
 193 parameterisation scheme that provides the right amount of mixing in the estuary. We have
 194 considered the parameterisation of horizontal eddy viscosity by Uittenbogaard et al. (1992), which
 195 is available in Delft3D-Flow and reproduces well the turbulent fluxes of momentum.

196 The best fit between results and simulations was obtained assuming the horizontal eddy
 197 diffusivity, K_h , to be in the range of $\sim[2-30] \text{ m}^2 \text{ s}^{-1}$ with small and large values applied respectively
 198 to small and large mesh cells. The sensitivity analysis for K_h , was conducted following Okubo
 199 (1971). Because Okubo's formula applies for open-water, it was observed that it was not properly
 200 simulating the true dispersion in the estuary, thus a factor f was used to increase and decrease
 201 mixing at the sub-grid scale (See Equation 2). Varying f allowed us to achieve the best fit between
 202 measurements and model results.

$$203 \quad K_h = f [2.05 \times 10^{-4} \times d^{1.15}] \quad (2)$$

204
 205 where d is the mesh cell size (from ~ 20 to ~ 300 metres), and f is the factor set to different values
 206 but only shown for 2, 100, 150, 200, 250, 400 and 2000 in the sensitivity analyses (see Table 3).

207 The *k-Epsilon* turbulent closure scheme was used to compute values for the vertical viscosity
 208 and diffusivity. We assumed the typical Manning roughness coefficient of $(0.02 \text{ m}^{-1/3} \text{ s})$, which
 209 characterises the higher percentage of local sediment (Souza et al., 2013). This resulted in a Chézy
 210 coefficient of $\sim 40 \text{ m}^{-1/2}/\text{s}$. Wind speed and directions, assumed to be **constant** over this small region,
 211 were obtained at the Caravelas station from the Instituto Nacional de Meteorologia INMET (code
 212 INMET 86764), at (source: <http://www.inmet.gov.br/portal/>), see Figure 4.

Preferred position for figure 4

213
214

215 The wind was assumed to only affect mesh cells in coastal areas. In other words, the wind
216 stress did not affect mesh cells inside the estuarine channels. Moreover, Andutta et al. (2013)
217 applied Hansen and Rattray's analytical equation of the velocity and salinity components, and
218 demonstrated that the wind effect in January 2008 was negligible at station C (near Nova Viçosa
219 estuarine mouth), which is the closest to the coast. Hansen and Rattray's analytical solution required
220 an adjustment of no more than 0.02 Pascal for the wind stress, which correspond to wind speeds of
221 $\sim 3 \text{ m s}^{-1}$ (Andutta et al., 2013). South-southwestward alongshore currents occur between October
222 and January, while north-northeastward alongshore currents are observed during the fall and winter
223 months Lessa and Cirano (2006).

224 Sea level data from TOPEX were used to force tides at the open boundary nodes. A time
225 series of water surface elevation from May to July 2007 was recorded at Terminal Aracruz (TA in
226 Figure 2), which is a few kilometers away from the coastal open boundary. At TA a total of
227 16,264 tidal measurements were recorded at five minute intervals, and were processed using the
228 tidal component extraction program PACMARÉ (Franco, 2000). These tidal measurements were
229 used to obtain the amplitude and phase of the main tidal components, shown in Table 2.
230 Additionally, sea-level data were recorded at stations A and C from 14th to 19th of January 2008,
231 and these data were used to validate modelled sea-level oscillation (comparison shown in Results
232 and Discussion section). Sea surface elevation observations from sites A and C showed the same
233 phase, strongly suggesting that tides propagate across the shelf, because tides propagating along the
234 coast would results in a phase shift between sea level observations at sites A and C (see Figure 2).
235 The measurements of tidal heights of $\sim 1 \text{ m}$ and $\sim 3 \text{ m}$ during neap and spring tides, respectively.
236 This ranks as meso-tidal, according to the criteria of Davies (1964) for tidal classification. From
237 the tidal heights shown in Table 3, the tidal form-number is $[N_f = (K_1 + O_1) / (M_2 + S_2) =$
238 $0.19]$, indicating a semidiurnal tidal estuary (Defant, 1960). The tidal components from Table 2
239 represent over 97% of sea level variations for the estuarine system (Andutta, 2011).

Preferred position for Table 2

240
241
242
243
244
245

d. Model validation criteria

In order to quantify the agreement between the simulated velocity and salinity profiles the method suggested by Wilmott (1981), based on the Skill parameter was used. Accordingly, the skill is measured as follows

$$Skill = 1 - \frac{\sum |X_{mod} - X_{obs}|^2}{\sum \left(|X_{mod} - \bar{X}_{obs}| + |X_{obs} - \bar{X}_{obs}| \right)^2}, \quad (3)$$

247 where X_{obs} and X_{model} denote the observational and simulated properties, respectively, \bar{X}_{obs} being
248 the mean observational values. The Skill parameter varies from 1 to zero, with 1 indicating the best
249 fit, and zero indicating a complete disagreement between observation and model results.

250
251

e. Modelling approach to calculate the Transport Timescales

252 To quantify the residence time and exposure time 35 thousand numerical particles were
253 released in the estuary by coupling D-Waq PART with results from the Delft3D-FLOW (i.e. within
254 the subdomain denoted ω). Numerical particles were deployed near the bottom and top layers. The
255 particle concentration using conservative tracer module was normalized to value 1 within the
256 volume of ω . Therefore, the number of particles decreases when particles exit ω , and increases
257 when particles re-enter ω . The minimal initial number of particles, i.e. 25 thousand, was computed
258 considering a minimum thickness of 2 m and a grid cell of ~20 by 10 meters.

259 A total of four simulation scenarios were made: (S_1) particle released at high water in neap
260 tide, (S_2) particle released at low water in neap tide, (S_3) particle released at high water in spring
261 tide, and (S_4) particle released at low water in spring tide.

262 In order to be consistent with CART timescales, for the computation of the residence time,
263 particles are discarded once they have reached an open boundary, e.g. estuarine head or an open

264 boundary in coastal waters (de Brauwere et al., 2011; de Brye et al., 2012). The arithmetic mean of
 265 the individual residence times, φ , was computed as the time necessary for particles to exit the
 266 domain (ω) for the first time. As for the exposure time, the particles are assumed to immediately
 267 bounce back into the domain only at estuarine heads. This simplifying hypothesis is unlikely to
 268 entail any major error, since a particle crossing the upstream estuarine boundary in the upstream
 269 direction (because of diffusive processes) will most likely return into the estuary after a relatively
 270 small time under the influence of the river flow, e.g., the St. Johans River in Florida, which
 271 experiences backflows over significant durations (Hendrickson et al., 2003).

272 Results from residence and exposure times were used to estimate the return coefficient
 273 distribution. The residence and exposure times may vary according to the time of release, such as
 274 during neap/spring tides or high/low tides, and this would also affect the return coefficient. This
 275 notwithstanding, results of exposure and residence times must be calculated for the same conditions
 276 when computing the return coefficient, i.e. $r = (\Theta - \varphi) / \Theta$.

277

278 *f. The modified LOICZ analytical model*

279 The modified LOICZ model of Andutta et al. (2014) applies the salinity balance proposed
 280 by Fischer et al. (1979) into the original formulation of the LOICZ. This water renewal timescale
 281 model has been shown to be sensitive to changes to some of its free parameters (e.g. river flow and
 282 salinity gradient). We expect that the estimates of the timescales from our numerical results would
 283 fit within the ranges derived from the LOICZ model. Details of its derivation are provided in
 284 Andutta et al. (2014); however we provide the simplified relation for water renewal timescale.

285

$$286 \quad \frac{1}{T_p} = \frac{1}{T_1} + \frac{1}{T_2}, \quad (4)$$

287

288 where $T_1 = L/U$ and $T_2 = L^2 / K$ are the advective and dispersive timescales, respectively. L , U , K
 289 and T_p are respectively the selected estuarine segment length, the flow speed, the characteristic
 290 value of the longitudinal diffusivity and the water renewal timescale. This expression may be re-

291 written in terms of the dimensionless Péclet number $Pe = ULK^{-1}$, the ratio $P_e = T_2/T_1$ of the
 292 dispersive to the advective timescale. Similarly, this number provides a comparison of contributions
 293 from advective and dispersive processes to transport timescales, yielding

294

$$295 \quad T_P = \frac{VP_e}{Q_R(1+P_e)}. \quad (5)$$

296 Where V and Q_R denote the estuarine volume and river discharge, respectively. The contribution of
 297 advection to the total water renewal timescale T_P , θ ($0 \leq \theta \leq 1$), is given by

$$298 \quad \theta = T_P/T_1 = Q_R/(Q_R + Q_D), \quad (6)$$

299

300

301

302 where Q_D is the discharge. Equations (4) and (6) were used to generate the advective-dispersive
 303 diagram (shown later), whose results will be compared to the numerical results.

304

305 *g. The CART analytical model*

306 As previously mentioned, in the framework of CART, the TTS that may be used to calculate
 307 water renewal rates can be obtained at any time and position as the solution of partial differential
 308 equations (Deleersnijder et al., 2006; de Brye et al., 2012; Andutta et al., 2014). For instance,
 309 residence time and exposure time were estimated using calibrated/validated numerical simulations
 310 for the Scheldt Estuary (de Brauwere et al. 2011, de Brye et al. 2012). As an easy acceptable
 311 method, analytical solutions may provide results that are representative of real situations (e.g.
 312 CART and LOICZ). The idealised CART timescales were used to obtain the exact analytical
 313 solution of the so called return coefficient for the ESCP. Different values of the Péclet number were
 314 considered, in order to assess the axial variation of return coefficient values. The advective
 315 timescale, $T_1 = V/Q_R$, and a dispersive timescale, $T_2 = P_EV/Q_R$, are defined taking into consideration
 316 the estuarine volume V . Andutta et al. (2014) provides a detailed description depicting an idealized
 317 channel for the time scales.

318 Consider an estuarine channel ($-\infty < x < \infty$) with a constant cross-sectional area A , and a
 319 flow under steady-state. The volumetric flow rate is denoted as Q_R . The downstream and upstream
 320 boundaries of our idealised estuary are located at $x = L_0$ and $x = L_1$, respectively. The estuarine
 321 length is $L = L_0 - L_1$, and thus the volume is $V = AL$. The water velocity is then
 322 $U = Q_R / A = LQ_R / V$. For the abovementioned conditions, the residence time satisfies the adjoint
 323 of the classical passive tracer transport equation (Delhez et al. 2004, Andutta et al. 2014), i.e.

324

$$325 \quad \frac{d}{dx} \left(AK \frac{d\varphi}{dx} + Q_R \varphi \right) = -A \quad (7)$$

326

327 where, x , denotes the particle position. The solution for the equation needs to satisfy the upstream
 328 and downstream boundary conditions,

329

$$330 \quad \varphi(L_1) = 0 = \varphi(L_0). \quad (8)$$

331

332 It represents the average time required by particles initially located in the interval $[x, x + \delta x]$
 333 (with $\delta x \rightarrow 0$) to reach one of the open boundaries. The solution is then easily derived:

334

$$335 \quad \varphi(x) = \frac{V}{Q_R} \left(1 - \frac{\xi}{L} \right) + \frac{V}{Q_R} \left(\frac{e^{-Pe} - e^{-Pe \xi/L}}{1 - e^{-Pe}} \right) \quad (9)$$

336 where $\xi = x - L_1$.

337 The exposure time was also derived (Andutta et al., 2014), and is defined in the domain of interest
 338 and its surrounding environment.

$$339 \quad -\infty \leq x \leq L_1 \quad : \quad \Theta(x) = \frac{V}{Q_R} \quad (10a)$$

$$340 \quad L_1 \leq x \leq L_0 \quad : \quad \Theta(x) = \frac{V}{Q_R} \left(1 - \frac{\xi}{L} \right) + \frac{V}{Q_R} \left(\frac{1 - e^{-Pe \xi/L}}{Pe} \right) \quad (10b)$$

$$341 \quad L_0 \leq x < \infty \quad : \quad \Theta(x) = \frac{V}{Q_R} \left(\frac{e^{-Pe} - 1}{Pe} e^{-Pe \xi/L} \right) \quad (10c)$$

342

343 From Equations (9) and (10), which are valid within the upstream and downstream open
 344 boundaries, the return coefficient is:

345

$$346 \quad r = \frac{\Theta(x) - \varphi(x)}{\Theta(x)} = \frac{\left(\frac{1 - e^{-Pe \zeta/L}}{Pe} \right) - \left(\frac{e^{-Pe} - e^{-Pe \zeta/L}}{1 - e^{-Pe}} \right)}{\left(1 - \frac{\zeta}{L} \right) + \left(\frac{1 - e^{-Pe \zeta/L}}{Pe} \right)} \quad (11)$$

347 Note that r is bounded by $[0,1]$, as mentioned before.

348 In principle, the residence time and the exposure time can be obtained by solving classical
 349 passive transport equations. However, to do so, time- and position-dependent concentrations must
 350 first be **obtained and**, then, time and space integral must be performed to derive the relevant
 351 timescales. This is not straightforward, even for highly idealised flows. This is why it is preferable
 352 to have recourse to the adjoint method established by Delhez et al. (2004), which requires the
 353 solution of simpler differential problems to be determined: in the present case, only ordinary
 354 differential equations are to be dealt with rather than partial differential ones. The disadvantage of
 355 this approach is that the theoretical underpinning of an adjoint model sometimes appears elusive,
 356 which is probably the reason why Errico (1997) wrote a general, enlightening paper on this matter,
 357 explaining the nature and purpose of adjoint models.

358

359 **3. Results and Discussion**

360

361 *a. Model calibration of salinity, velocity and tides*

362 We carried out a sensitivity analysis considering different values for the horizontal diffusion
 363 coefficient k_h using Equation 2. These adjustments of factor f for the horizontal diffusivity based on
 364 the grid size allowed us to obtain a proper representation of the salinity field and its time variability.

365

Preferred position for Table 3

366 The mean Skill parameters for the simulation are shown in Table 3 for different values of
367 factor f , which was described with Equation 2. The comparison of sea-level oscillation over a tidal
368 modulation period, from the 14th to the 29th of January 2008, showed good skill values for locations
369 A (Figure 5) and C (not shown), and the Skill parameter for tides was calculated to be over 0.97 for
370 both locations, i.e. A and C. The comparison of tides, velocity, and salinity showed good skill
371 values during spring tides (not shown), and reasonable values during neap tides (Figure 6).

372
373
374
375

Preferred position for figure 5
Preferred position for figure 6

376 The Skill parameter for the water column height variation in time was calculated to be over
377 0.98 for all the sites under neap and spring tides (Table 4), and the tidal ranges were ~1.0 m and
378 ~2.5 m for neap and spring tides, respectively. Observations have shown that the tidal phase
379 between sites A (Caravelas mouth) and C (Peruípe mouth) is almost the same. The similarity of
380 their phases indicates that tides propagate mainly perpendicular to the coast line in this region, a
381 result which is in close agreement with observations previously reported by Lessa and
382 Cyrano (2006).

383 For the modeled velocity validation, good results (Skill from 0.77 to 0.93) were obtained in
384 spring tides in the estuaries of Caravelas (sites A and B) and Nova Viçosa (sites C and D). For neap
385 tides due to small differences on tidal asymmetry, the Skill was lower, at ~ 0.6.

386 The model agreed well with observations of maximum ebb and flood currents at site A. The
387 model also properly simulated the velocity profiles for sites B, C, and D. Therefore, the description
388 of maximum ebb and flood currents from in-situ data also apply to the model simulations. At site B
389 there were maximum speeds of ~0.5 m s⁻¹ and 1.0 m s⁻¹ (ebb events), and ~-0.3 m s⁻¹ and ~-0.6 m s⁻¹
390 (flood events), during neap and spring tides, respectively. For site A the vertical shear of the
391 velocity was negligible in flood and ebb conditions, while for site B there was a small vertical shear
392 of the horizontal velocity during ebb events. During flood events, the water velocity was
393 homogenous over the water column. In addition, a residual velocity of ~0.05 m s⁻¹ was calculated at

394 site B, indicating a residual circulation from Nova Viçosa towards the Caravelas River. Site A had a
395 residual current of $\sim 0.06 \text{ m s}^{-1}$, indicating a small discharge from the Cupído and Jaburuna Rivers.
396 At sites C and D, located in the Peruípe River, the downstream velocities showed more intensity
397 than observed in the Caravelas Channel. For site C the downstream velocities varied from $\sim -0.9 \text{ m}$
398 s^{-1} to $\sim -1.5 \text{ m s}^{-1}$, for neap and spring tides, respectively. During flood events, the velocities were \sim
399 0.3 m s^{-1} and $\sim -0.7 \text{ m s}^{-1}$, for neap and spring tides, respectively. At site D the maximum
400 downstream velocities were only $\sim 0.7 \text{ m s}^{-1}$ and $\sim 1.0 \text{ m s}^{-1}$ at neap and spring tides, and upstream
401 velocities were $\sim -0.3 \text{ m s}^{-1}$ and $\sim -0.4 \text{ m s}^{-1}$. The residual velocities at sites C and D, which have
402 values of $\sim 0.10 \text{ m s}^{-1}$ to $\sim 0.15 \text{ m s}^{-1}$, indicate a higher advective contribution from the Peruípe River
403 compared with the Caravelas estuary.

404 In addition to the tides and the velocity field, the model simulated the temporal variation of
405 the salinity well for all sites (A, B, C, and D). During spring tides the calculated Skill values were
406 over 0.83, while for neap tides they were over 0.73 (Table 4). At the Caravelas estuarine channel,
407 $\sim 3 \text{ km}$ near the mouth (site A), during low tide, salinity was observed in intervals of $\sim 34.5 \text{ psu}$ to
408 $\sim 35.0 \text{ psu}$ and $\sim 34.0 \text{ psu}$ to $\sim 34.5 \text{ psu}$ for the observational and theoretical results,
409 respectively. About 6 km away from the mouth we obtained a good agreement for the salinity, with
410 $\sim 32.0 \text{ psu}$ and $\sim 32.5 \text{ psu}$ for observation and simulation, respectively. In the vicinity of the
411 interconnection with Cupído and Jaburuna Rivers (site B), which is about 12 km upstream from the
412 mouth, the salinity decreased to $\sim 30.0 \text{ psu}$ and $\sim 28.5 \text{ psu}$ for the observational and calculated
413 results, respectively. At high tide, near the mouth (site A) and at a distance of 6 km from the mouth,
414 the salinity was $\sim 36.5 \text{ psu}$ and $\sim 36.0 \text{ psu}$, respectively, for both simulation and field measurements.
415 In the upper reaches of the estuary, near the junction of the rivers, Cupído and Jaburuna ($\sim 12 \text{ km}$
416 from the mouth), a close agreement between simulated and observed salinity values ($\sim 33.0 \text{ psu}$) was
417 obtained at high tide. Along the Peruípe River estuary at neap tides, the surface salinities vary in the
418 range of 20.0 psu to 34.0 psu at the surface, and 32.5 psu to 36.0 psu near the bottom. The region of
419 Nova Viçosa has more vertical stratification of the salinity than at sites A and B in the Caravelas

420 River. This is due to Peruípe River's larger freshwater discharge. The observed value of ~36.0 psu
421 near the bottom is characteristic of the Tropical Water Mass, which was already reported to enter
422 this estuarine system (Schettini et al., 2010). During spring tides the vertical mixing causes the
423 erosion of the halocline, and thus decreases vertical stratification. This results in a smaller vertical
424 variation of 31.0 psu to 36.0 psu from the surface to the bottom.

425 **Preferred position for Table 4**

426 A comparison of the axial distribution of salinity was made for the Caravelas River (Figure
427 7A,B). For the first 12 km along the estuarine channel, results from simulations were compared to
428 observations made by Schettini and Miranda (2010). The measurements were obtained on the 10th
429 of April, 2001 during spring tides. Although the field data are likely to be from different conditions
430 of river flow, the simulation showed a good correlation of the axial distribution of the salinity in the
431 Caravelas River (See Figures 7C and 7D), with values of $R^2 \sim 0.97$ and $R^2 \sim 0.99$ for low and high
432 tides respectively. This indicates that the model has well represented the mixing processes in the
433 Caravelas Estuary. During low tide (Figure 7A,C), a good agreement is found near the mouth, with
434 salinity values of ~35.2 psu and ~ 34.5 psu, for the model results and observations, respectively. At
435 nearly 6 km upstream, there is still a good agreement ($R^2 \sim 0.99$) with the salinity values of ~33
436 psu (model), and ~32 psu (observation). Further upstream and near the inter-connection between the
437 Cupído and Jaburuna rivers (i.e. ~ 12 km upstream), the agreement is slightly poorer with the
438 salinity values of ~30 psu (model) and ~29 psu (observation). At high tide (Figure 7B, D), the
439 model predicted the longitudinal salinity variations well along the Caravelas Channel. The salinity
440 values near the mouth were ~36.4 psu (model and observation), and reduced to ~36 psu 6 km
441 further upstream. Moreover, during high tides the agreement was also good near the channel
442 between the Cupído and Jaburuna rivers with salinity of ~33 psu.

443 **Preferred position for figure 7**

444
445 *b. Results of the residence time, the exposure time and the return coefficient*

446

447 The transport timescales, namely residence time (φ), exposure time (Θ), and the return
448 coefficient (r), were estimated for the Caravelas and Peruípe estuarine channels with simulation
449 under different scenarios, i.e. S₁ to S₄ (Figures 8, and 9).

450 For scenarios S₁ and S₃ (Figure 8), the residence time along the Caravelas Channel, from the
451 mouth to 12 km upstream, was found to vary from 0 to ~15.0 days. The inflow boundaries of the
452 Cupído and Jaburuna rivers were found to have residence times of ~27 and ~22 days, respectively.
453 For the Peruípe Channel the residence times ranged from 0 to ~7.4 days, from the mouth to 5 km
454 upstream, with a maximum value of ~18 days at the inflow boundary of the Peruípe Estuary.

455 The residence time estimated at ~6 km further upstream in the Caravelas Estuary ($\varphi = 11.7$
456 days) is almost three times larger than the residence time calculated for the same distance along the
457 Peruípe Estuary ($\varphi < 4.4$ days). The difference between results in the Caravelas and the Peruípe
458 estuaries is due to the larger velocity contribution in the Peruípe Estuary.

459 Comparing scenarios S₁ and S₃, the residence time was found to be slightly lower for S₃ (c.a.
460 a few hours) and this difference is due to increased diffusive contribution during stronger spring
461 tidal conditions. In contrast to scenarios S₁ and S₃, the simulations considering scenarios S₂ and S₄
462 yielded an increased residence time. This increase was maximum near the estuarine mouths (~5
463 days), and observed to reduce in the upstream direction (few hours). The increase in residence time
464 for particles released in slack water of low tide is caused by tidal excursion from reversing currents
465 (i.e. flood currents). These results reflect and add value to recent simulations by de Brye et al.
466 (2012) for the Scheldt Estuary (in Belgium and the Netherlands), whose results showed larger
467 residence time values for particles released at slack water of low tides than for high tides (difference
468 of a few days).

469 The virtual Lagrangian particles showed that a negligible number of particles crossed the
470 connecting channel between the Caravelas (ω_1) and Peruípe Estuaries (ω_2), which indicates that this
471 relatively narrow and shallow interconnection channel allows little exchange of water properties
472 between these estuaries. Moreover, the residence time is observed to be larger within the

473 enlargement of the interconnecting channel between these two estuaries. Schettini and Miranda
 474 (2010) and Schettini et al. (2013) have addressed the importance of the interconnection channel
 475 between Caravelas and Peruípe, and found that sediment deposited near the Caravelas mouth was
 476 both inner shelf **local resuspension** and upstream transport, or sourced from the Peruípe River via
 477 the interconnection channel.

478 **Preferred position for figure 8**

479
 480
 481 Exposure time results showed that particles re-entered the system for up to two days (Figure
 482 9). Note that the difference between the exposure time and the residence time ($\Theta - \varphi$) showed little
 483 spatial variation for scenarios S_1 and S_3 .

484 **Preferred position for figure 9**

485
 486 The spatially averaged difference between exposure and residence times ($\Theta - \varphi$) are
 487 calculated in days, and its respective RMSE to be $\sim 1.98 \pm 0.06$ for S_1 , $\sim 1.87 \pm 0.12$ for S_2 , ~ 1.92
 488 ± 0.07 for S_3 , $\sim 2.19 \pm 0.08$ for S_4 . These results strongly suggest that ($\Theta - \varphi \sim \text{const.}$) for the
 489 ESCP under the four different scenarios considered. The results also suggest that $t_3 - t_2$ varies little
 490 away from the open boundaries, so particles deployed at different times and locations in the estuary
 491 re-enter for similar lengths of time, assuming the circulation in coastal waters does not considerably
 492 change over time due to additional forcings, e.g. sudden alongshore wind driven currents.

493 Equation (5) was used to estimate the range of water renewal timescales for the Caravelas
 494 and Peruípe estuaries using the parameters given in the appendices of Andutta et al. (2014), see
 495 Figure 10. The straight line labelled θ (lowercase) indicate the relative advective contribution to
 496 water renewal, where $0 \leq \theta \leq 1$. The line at $\theta = 0.5$ separates the areas where transport is
 497 dominated by advection (diagram upper zone, $\theta > 0.5$) and dispersion (diagram lower zone, $\theta <$
 498 0.5).

499 The Caravelas and Peruípe estuaries have mean depths of ~ 6.5 and ~ 7.5 meters,
 500 respectively, and the maximum and minimum tidal ranges in these estuaries are ~ 2.5 and ~ 0.5

501 meters. According to Andutta et al. (2013), these tidal ranges combined with the relatively the small
502 depths result in a high rate of change of the potential energy ($\sim 6.1 \text{ J m}^{-3} \text{ s}^{-1}$), which contributes
503 towards large dispersion. It is valid to compare these results to the Sheldt Estuary, where tidal
504 oscillation is typically 4-5 meters along the first ~ 100 km, and where the mean water depth is ~ 10
505 meters. Tidal range in the Sheldt can reach ~ 7 m, which is about 45% of the mean water depth
506 value for the first ~ 25 km near the estuarine mouth (Soertaert and Herman, 1995; de Brye et al.
507 2012), and this system is classified as well-mixed due to dispersion prevailing over advection. The
508 numerical results for the ESCP fit within the timescale ranges estimated using the simple LOICZ
509 method.

510
511
512

Preferred position for figure 10

513 The return coefficient cannot be calculated using the modified LOICZ model. However, it
514 was computed numerically and compared to the non-dimensional solution obtained using CART.
515 The return coefficient converges to one at the estuarine mouths and near estuarine heads (Figure 11,
516 for all scenarios S_1 to S_4 and Figure 12B). However, this is only a direct consequence of the
517 definition of the residence time, which converges to zero at the entrance, and thus the return
518 coefficient will always increase towards unity. r was observed to be smaller upstream, because the
519 ratio $(\Theta - \varphi)/\Theta$ is likely to decrease. It can be noticed that the axial variation of the return
520 coefficient is similar for both CART solution and numerical approach (Figures 11 and 12C). The
521 return coefficient calculated from CART and from numerical simulations is observed to increase
522 towards the upstream boundary. This increase towards the estuarine head is due to the boundary
523 condition assumed in the analytical and numerical solutions, where particles do not re-enter the
524 domain after crossing the estuarine head, although in a real estuary water particles would re-enter
525 through the estuarine head due to river flow conditions.

526 Figure 12A shows results of the residence and exposure time and return coefficient for a
527 range of values of the Péclet number. High values of the Péclet number yield a boundary layer in
528 the vicinity of the upstream location.

529 The greater the relative importance of advection, the less likely it is that dispersion will
530 cause a water particle to hit the upstream boundary of the domain ($x = L_0$). In accordance with their
531 definitions, the exposure time is larger than the residence time for any location in the domain ($L_1 \leq$
532 $\xi/L \leq L_0$). These idealised results of the return coefficient were used to access results obtained
533 from our numerical simulations.

534

535
536 **Preferred position for figure 11**
537

538 **Preferred position for figure 12**
539

540 In the illustration shown in Figure 11A, the ratio is simply the difference between times t_3
541 and t_2 . Evidently this is a simple case where the particle is assumed to have re-entered the domain
542 only once.

543 Particles are expected to first cross the estuarine mouth during ebb currents, which would be
544 alternating with flood currents and dispersive processes. Therefore, we could presume that
545 Lagrangian particles would have a time window of ~ 6.5 hours to cross the entrance (for semi-
546 diurnal tidal estuaries), and this time window would then close for ~ 6.5 hours (the period of flood
547 currents).

548 Our simulations were for relatively calm weather conditions, which were predominant over
549 the region, c.a. wind speeds in the range $1-4 \text{ m s}^{-1}$ (wind from NE). Andutta et al. (2013) showed
550 that wind conditions did not affect the water circulation in this estuarine system in January 2008.
551 However, for stronger wind conditions the results would not be the same. Evidently alongshore
552 wind-driven currents would reduce the difference between the exposure time and the residence
553 time, and the return coefficient would thus decrease towards zero. This is because alongshore
554 currents inhibit the propensity of particles to re-enter the estuarine system. The alongshore shelf
555 currents are observed to be driven by the N-S migration of the South Atlantic High between
556 summer and winter. South-southwestward alongshore currents occur between October and January,
557 while stronger north-northeastward alongshore currents are observed during the fall and winter
558 months (Lessa and Cirano, 2006).

559

560 **4. Conclusions**

561

562 *Overall goal*

563 This study provides the first estimates of the residence time, exposure time and the return
564 coefficient for the Caravelas and Peruípe estuaries and might be a reference for future studies
565 related to **the control of pollutants and sediment transport**. These transport timescales were
566 estimated using a Lagrangian model only as a tool, and this model has been properly calibrated and
567 validated using field data.

568 *Specific conclusions*

569 • *Achievements regarding goals (1 and 2)*

570 The residence time for particles released far upstream in the Caravelas Estuary was found to
571 be nearly 3 weeks for particles, regardless of whether they are released at high or low tide, and is
572 driven by tidal dispersion combined with the discharge from the Cupído and Jaburuna Rivers
573 (typical range of 4 to 9 m³ s⁻¹). These results are consistent with previous estimates derived from
574 simple analytical solutions (Andutta et al., 2014), see Figure 10. For the Peruípe Estuary, our
575 estimates of the residence time were for less than one week, due to the tidal dispersion combined
576 with the larger river input from the Peruípe River (typical range of 20 to 70 m³ s⁻¹).

577 The transport timescales (exposure and residence times) were found to be quite similar for
578 particles released in high tide under spring and neap tidal conditions, thus confirming previous
579 estimations made for the Scheldt Estuary (de Brye et al., 2012). In contrast, the transport timescales
580 were shown to be more sensitive to tidal-phase release time (i.e. high or low tides) in this estuarine
581 system. Similar observations were made for the Scheldt Estuary (de Brauwere et al., 2011), in
582 which there was a difference of days for results of residence time using particles released at high
583 and low tides. This suggests that tidal-phase release time for a meso-tidal shallow estuary forced by
584 low-moderate river discharge conditions is important for quantification of TTS, especially for water
585 particles near mouths where larger tidal excursions are expected compared to locations further
586 upstream, and since their initial movement would be upstream/downstream if released during
587 low/high tide, respectively.

588 The Lagrangian simulation also showed that the narrow and shallow inter-connecting
589 channel between the Peruípe and Caravelas estuaries allows **little** water exchange between the two
590 estuaries, and only a few particles were capable of crossing the inter-connection passage with
591 prevailing direction from the Peruípe to the Caravelas, in agreement with Schettini et al. (2013).
592 Therefore, both exposure time and residence time were large at that location, and the exchange of
593 water properties is likely to happen through alongshore currents at inner coastal areas.

594 • *Achievements regarding goal (3)*

595 Similarly to the exposure and residence times, the return coefficient was shown to be more
596 sensitive to tidal phase (high and low tide), than to neap and spring tidal conditions. It may be
597 summarized as follows: (1) the return coefficient is larger for particles released at high tide than at
598 low tide; (2) the return coefficient is larger for particles released during spring tides than during
599 neap tides.

600 For these two estuaries the exposure time was higher than the residence time in all
601 simulations, thus showing that water may return to the system after having first crossed the mouth.
602 The propensity of this water to return to the estuary was quantified using the return coefficient,
603 which depends on the difference between the exposure and residence times, and thus also on the
604 residual circulation due to river discharge, as well as the circulation in coastal waters. For instance,
605 swift longshore currents decrease the difference between the exposure and residence times, and
606 therefore reduce the return coefficient. The wind conditions over our measurement period were
607 characteristic of calm weather, c.a. a few m s^{-1} (see Figure 4), and different scenarios may produce
608 different results for the transport timescales, for **instance** under stronger north-northeastward
609 alongshore currents which are often observed during the fall and winter months Lessa and Cirano
610 (2006). Due to its definition, the return coefficient is predicted to be larger at the estuarine mouths,
611 because the residence time tends to zero (see Equation 1). Our results have additionally shown that
612 for our scenarios the difference between exposure and residence times ($\Theta - \varphi$) is nearly constant
613 within our domain. This can also be observed from our analytical solution (Figure 12C).

614

615 **6. Acknowledgements**

616

617 We acknowledge the Conselho Nacional de Desenvolvimento Científico e Tecnológico
618 (CNPq) grant 420219/2005-6 to Eurico Cabral de Oliveira, and the fellowships (Procs. LBM-
619 302069/2004-6, CAFS-306217/2007-4 and ES-308303/2006-7). We also acknowledge the
620 assistance in the field work from Carlos A. F. Schettini, Eduardo Siegle, Mario Pereira, Piero L. F.
621 Mazzini, Vitor M. Izumi, and the collaboration of other graduate students and technicians of the
622 Dept. of Physical, Chemistry and Geology of IO-USP, PPGGeo/UFRGS and UFRN. Eric
623 Deleersnijder is an honorary Research Associate with the Belgian Fund for Scientific Research
624 (F.R.S.-FNRS).

625

626 **References**

627

- 628 Andutta, F.P., Ridd, P.V., Deleersnijder, E., Prandle, D., 2014. Using field data for estimating
629 estuarine water transport timescales and the associated return coefficient. *Progress in*
630 *Oceanography* 120, 139–153, doi: 10.1016/j.pocean.2013.08.009.
- 631 Andutta, F.P., Miranda, L., Schettini, C.A.F., Siegle, E., da Silva, M.P., Izumi, V.M., Chagas, F.M.,
632 2013. Temporal variations of Temperature, Salinity and circulation in the Peruípe River
633 Estuary (Nova Viçosa, BA). *Continental Shelf Research* 70, 36–45, doi:
634 10.1016/j.csr.2013.03.013.
- 635 Andutta, F.P., 2011. The estuarine system of the Caravelas and Peruípe rivers (Bahia):
636 Observations, simulations, residence time, and advective and diffusive processes, PhD Thesis.
637 IO-USP, Oceanography Institute of the University of São Paulo, 121 pp.
- 638 Chaves, F.O., Soares, M.L.G., Estrada, G.C.D., Cavalcanti, V.F., 2009. Maintenance of mangrove
639 forest through the conservation of coastal ecosystems. *Journal of Coastal Research* 56, 395–
640 399.
- 641 Costa Jr., O.S., Leão, Z.M.A.N., Nimmo, M., Attrill, M.J., 2000. Nutrifcation impacts on coral
642 reefs from northern Bahia, Brazil. *Hydrobiologia* 440, 307–315, doi:
643 10.1023/A:1004104118208.

- 644 Defant, A., 1960. *Physical Oceanography*, Pergamon Press, New York 2, 598 pp.
- 645 Deleersnijder, E., Beckers, J.-M., Delhez, E.J.M., 2006, On the behaviour of the residence time at
646 the bottom of the mixed layer, *Environmental Fluid Mechanics* 6, 541–547.
- 647 Delft Hydraulics, 2008. *Delft-3D Flow Manual*, Delft Hydraulics, Delft, Holanda, 674 pp.
- 648 Delhez, E.J.M., Heemink, A.W., Deleersnijder, E., 2004. Residence time in a semi-enclosed domain
649 from the solution of an adjoint problem, *Estuarine, Coastal and Shelf Science* 61, 691–702.
- 650 Delhez, E.J.M., de Brye, B., de Brauwere, A., Deleersnijder, E., 2014. Residence time vs influence
651 time. *Journal of Marine System* 132, 185–195, doi: 10.1016/j.jmarsys.2013.12.005.
- 652 de Brauwere, A., de Brye, B., Blaise, S., Deleersnijder, E., 2011. Residence time, exposure time and
653 connectivity in the Scheldt Estuary. *Journal of Marine Systems* 84, 85–95, doi:
654 10.1016/j.jmarsys.2010.10.001.
- 655 de Brye B., de Brauwere, A., Gourgue, O., Delhez, E.J.M., Deleersnijder, E., 2012, Water renewal
656 timescales in the Scheldt Estuary, *Journal of Marine Systems* 94, 74–86.
- 657 Errico, R.M., 1997, What is an adjoint model?, *Bulletin of the American Meteorological Society*,
658 78, 2577-2591.
- 659 Fischer, H.B., List, E.Y., Koh, R.C.Y., Imberger, J., Brooks, N.H., 1979. *Mixing in Inland and*
660 *Coastal Waters*. Academic Press, New York, 483 pp.
- 661 Franco, A.S., 2000. *Mares: Programa para previsão e análise*. Manual, BSP, São Paulo, 36pp.
- 662 Gaeta, S.A., Lorenzetti, J.A., Miranda, L. B., Susini-Ribeiro, S.M.M., Pompeu, M., Araujo, C.E.S.,
663 1999. The Vitoria Eddy and its relation to the phytoplankton biomass and primary
664 productivity during the austral fall of 1995. *Brazilian Archive of Fishery and Marine Research*
665 47(2-3), 253–270.
- 666 Hendrickson, J.C., E.F. Lowe, D. Dobberfuhl, P. Sucsy, and D. Campbell. 2003. Characteristics of
667 Accelerated Eutrophication in the Lower St. Johns River Estuary and Recommended Targets
668 to Achieve Water Quality Goals for the Fulfillment TMDL and PLRG Objectives. Department
669 of Water Resources, St. Johns River Water Management District, Palatka, Florida.
- 670 Holzer, M., Hall, T.M., 2000. Transit-time and tracer-age distributions in geophysical flows.
671 *Journal of the Atmospheric Sciences* 57, 3539–3558.
- 672 Ketchum, B.H., 1951. The exchanges of fresh and salt water in tidal estuaries. *Journal of Marine*
673 *Research* 10, 18–38.
- 674 Knoppers, B., Ekau, W., Figueredo, A. G., 1999. The coast and shelf of east northeast Brazil and
675 material transport. *Geo-Marine Letters* 19, 171–178, doi: 10.1007/s003670050106.
- 676 Leipe, T., Knoppers, B., Marone, E., Camargo, R., 1999. Suspended matter transport in coral reef
677 waters of the Abrolhos bank Brazil. *Geo-Marine Letters* 19, 186–195, doi: 1
678 0.1007/s003670050108.

- 679 Lessa, G.C., Cirano, M., 2006. On the circulation of a coastal channel within the Abrolhos Coral-
680 Reef system-Southern Bahia, Brazilian Journal of Coastal Research 39, 450–453.
- 681 Monsen, N.E., Cloern, J.E., Lucas, L.V., Monismith, S.G., 2002. A Comment on the Use of
682 Flushing Time, Residence Time, and Age as Transport Time Scales, Limnology and
683 Oceanography 47, 1545–1553.
- 684 Okubo, A., 1971. Diffusion Diagrams, Deep-Sea Research 18, 789–802, doi: 10.1016/0011-
685 7471(71)90046-5.
- 686 Pereira, M.D., Siegle, E., Miranda, L.B., Schettini, C.A.F., 2010. Hidrodinâmica e transporte de
687 material particulado em suspensão sazonal em um estuário dominado por maré: estuário de
688 Caravelas (BA), Revista Brasileira de Geofísica 28(3), 427–444, doi: 10.1590/S0102-
689 261X2010000300008.
- 690 Schettini, C.A.F., Pereira, M.D., Siegle, E., Miranda, L.B., Silva, M.P., 2013. Residual fluxes of
691 suspended sediment in a tidally dominated tropical estuary. Continental Shelf Research 70
692 (SI), 27–35, doi: 10.1016/j.csr.2013.03.006.
- 693 Schettini, C.A.F., Miranda, L.B., 2010. Circulation and Suspended Matter Transport in a Tidally
694 Dominated Estuary: Caravelas Estuary, Bahia, Brazil. Revista Brasileira de Oceanografia 58,
695 1–11, doi: 10.1590/S1679-87592010000100001.
- 696 Sheldon, J.E., Alber M., 2006. The Calculation of Estuarine Turnover Times Using Freshwater
697 Fraction and Tidal Prism Models: A Critical Evaluation. Estuaries and Coasts 29, 133–146.
- 698 Smagorinsky, I., 1963. General circulation experiment with Primitive equations. Monthly Weather
699 Review 91, 91e164.
- 700 Summerhayes, C., Melo, U.D., Barreto, H., 1976. The influence of upwelling on suspended matter
701 and shelf sediments off southeastern Brazil, Journal of Sedimentary Petrology 46, 819–828.
- 702 Teixeira, C.E.P., 2006. Caracterização e variabilidade da hidrodinâmica da zona costeira adjacente
703 ao banco de Abrolhos, MSc Thesis. IO-USP, Oceanography Institute of the University of São
704 Paulo, 93 pp.
- 705 Uittenbogaard, R. E., J. A. T. M. van Kester and G. S. Stelling, 1992. Implementation of three
706 turbulence models in 3D-TRISULA for rectangular grids. Tech. Rep. Z81, WL j Delft
707 Hydraulics, Delft, The Netherlands.
- 708 Wilmott, C. J., 1981. On the validation of models, Physical Geography 2, 184–194.
- 709 Zimmerman, F., 1988. Estuarine residence times, in B. Kjerfve (Ed.), Hydrodynamics of estuaries,
710 vol. 1, pp. 75–84, CRC Press.

711

712

1 **An assessment of transport timescales and return coefficient in adjacent tropical estuaries**

2 FERNANDO P. ANDUTTA^{a,b*}, FERNANDA HELFER^a, LUIZ BRUNER DE MIRANDA^b, ERIC

3 DELEERSNIJDER^{c,d}, CHRISTOPHER THOMAS^e, CHARLES LEMCKERT^a

4 ^a Griffith School of Engineering, Griffith University, Gold Coast, QLD 4222, Australia.

5 ^b Oceanographic Institute, University of São Paulo, São Paulo SP, Brazil, CEP 05508-900, Brazil.

6 ^c Université catholique de Louvain (UCL), Institute of Mechanics, Materials and Civil Engineering
7 (IMMC) & Earth and Life Institute (ELI), 4 Avenue Georges Lemaître, Bte L4.05.02, B-1348
8 Louvain-la-Neuve, Belgium

9 ^d Delft University of Technology, Delft Institute of Applied Mathematics (DIAM), Mekelweg 4,
10 2628CD Delft, The Netherlands

11 ^e Université catholique de Louvain (UCL), Institute of Mechanics, Materials and Civil
12 Engineering (IMMC), 4 Avenue Georges Lemaître, Bte L4.05.02, B-1348 Louvain-la-Neuve,
13 Belgium.

14

15 **Abstract –**

16 Transport timescales (TTS), namely residence time and exposure time, were computed for adjacent
17 shallow meso-tidal tropical estuarines system using the Lagrangian model D-Waq Part coupled with
18 the hydrodynamic model Delft3D-Flow, and the Constituent-oriented Age and Residence time
19 Theory, CART. The main results are threefold: **(a)** The TTS differs more between releases at high
20 or low tide than between those at spring and neap tides. The exposure time was also calculated and
21 found to be larger than the residence time by a few days. **(b)** The exposure and residence times were
22 used to evaluate the return coefficient (r) for different scenarios. As with residence and exposure
23 times, the return coefficient was found to differ more between releases at high or low tide than
24 between those at spring and neap tides. **(c)** For the Caravelas Estuary, where the river inflow was
25 low ($\sim 4 \text{ m}^3 \text{ s}^{-1}$), the residence time was found to be much larger than for the Peruípe Estuary, where
26 the river discharge was greater and nearly constant during the sampling period ($\sim 20 \text{ m}^3 \text{ s}^{-1}$). These
27 results shows the importance of advection in decreasing TTS in the Peruípe Estuary compared to
28 the Caravelas Estuary. The influence of the advection and dispersion agrees with previous simple
29 estimates obtained using the newly modified Land Ocean Interaction Coastal Zone (LOICZ) model
30 by Andutta et al. (2014).

31

32 Keywords: tropical estuary; residence time; exposure time; return coefficient; numerical model;
33 hydrodynamics.

34

35 **1. Introduction**

36 Since the dynamics of most estuarine systems is relatively complex, studies of transport
37 timescales (TTS) provide valuable insight into estuarine behaviour. Transport timescales represent a
38 more holistic way of interpreting the flow in complex systems (e.g. Monsen et al. 2002), and allow
39 us to understand how advective and dispersive mechanisms transport water.

40 Transport timescales are driven by the water currents, which in turn are influenced by sea
41 level oscillation, bathymetry and the temperature and salinity fields. It is therefore necessary to have
42 an accurate representation of these quantities in order to satisfactorily estimate transport timescales.

43 This article has the following tasks:

44 (1) to demonstrate, using a 3D hydrodynamic model combined with particle simulations,
45 how release times (e.g. slack waters of high and low tides, neap and spring tides) affect the
46 exposure time and residence time in a shallow meso-tidal tropical estuary.

47 (2) to compare TTS results from numerical modelling with estimates using the simple
48 newly modified Land Ocean Interaction Coastal Zone (LOICZ) model by Andutta et al. (2014).

49 (3) to calculate and evaluate the return coefficient (r) numerically and analytically using
50 CART. This is a measure of the propensity of a water parcel to return into the domain of interest
51 after leaving it.

52

53 *a. Overview of Transport Timescales*

54 Since the pioneering work by Ketchum (1951) and Bolin and Rodhe (1973), the theory of
55 TTS has evolved (e.g. CART, www.climate.be/cart), and other TTS definitions have been
56 introduced in order to fill scientific gaps. Therefore, there are many different transport timescale
57 definitions, e.g. flushing time (Ketchum, 1951; Fischer et al., 1979; Monsen et al., 2002), residence

58 time (Bolin and Rodhe, 1973; Monsen et al., 2002; Delhez et al. 2004; Deleersnijder et al., 2006),
 59 exposure time (Monsen et al., 2002), transit time (Holzer and Hall 2000), influence time (Delhez et
 60 al., 2014), age (Bolin and Rodhe, 1973; Monsen et al., 2002), e-folding flushing time (Monsen et
 61 al., 2002), turnover time (Sheldon and Alber, 2006) and renewal time (Andutta et al., 2014) – all of
 62 which have their own interpretation.

63 Two timescales, residence time and exposure time, are used to provide an indication of
 64 increase or decrease of non-reactive and reactive substances in estuaries, bays, lagoons, and atolls
 65 (Andutta et al., 2014). The residence time (Θ) is the time needed for a particle constituent to reach
 66 for the first time an open boundary of the domain of interest (e.g. Delhez et al., 2004). The exposure
 67 time (φ) is the time the particle will stay in the domain (e.g. Monsen et al., 2002) (Figure 2).
 68 Therefore, at a given time and location, the exposure time is always larger than or equal to the
 69 residence time. The larger the difference between the two timescales, the more often the particles
 70 tend to re-enter the domain of interest after leaving it for the first time. To evaluate the exposure
 71 time, the computational domain must be larger than the domain of interest (de Brauwere et al.,
 72 2011, de Brye et al., 2012). Estimates of these timescales may be obtained in an Eulerian or a
 73 Lagrangian framework. The latter often requires sufficiently large number of numerical particles in
 74 order to provide a result that statistically approaches the real condition.

75 A dimensionless return coefficient, r , represents the propensity of particles to return into the
 76 estuary after reaching an open boundary for the first time, as illustrated in Figure 1A (de Brauwere
 77 et al., 2011). It is defined as the relative difference between φ and Θ , i.e.

$$78 \quad r = \frac{(\Theta - \varphi)}{\Theta} . \quad (1)$$

79 Clearly, this coefficient lies in the interval [0,1].

80 The larger the r the more likely it is that particles will re-enter the estuary after crossing one
 81 of its open boundaries for the first time. Accordingly, particles that never return into the estuary
 82 have $r = 0$, while particles returning often or for long periods of time have r close to unity.

83
84
85
86

Preferred position for figure 1

87 *b. Chosen estuary and coastal area*

88 The domain of interest is the estuarine System of the Caravelas and Peruípe Rivers (ESCP),
89 in southern Bahia state, Brazil (see Figure 2); more details may be found in Appendix 1. It is
90 located at the approximate latitude of 17°50'S, nearly 60 km from the National Maritime Park of
91 Abrolhos, which is one of the largest reef structures of the Atlantic ocean, providing habitat for
92 innumerable marine species. The ESCP has two main mouths: the Caravelas Estuary in the north
93 (17°45'S), with two small channels named Barra Velha (~1 km wide) and Tomba's Mouth (~600 m
94 wide), and the Peruípe Estuary in the south (17°54'S) with a funnel shape ranging in width from
95 ~3500 m to ~700 m in the first few hundred meters. These two mouths are separated by a distance
96 of ~25 km alongshore, and are internally connected by shallow and narrow channels around
97 Cassurubá or Cassumba Island. Our simulations consider the domain shown in Figure 1C, for which
98 results were computed according to the number of particles in the control domain with boundaries
99 ω_1 and ω_2 .

100

101

102

103

Preferred position for figure 2

104 **2. Methods**

105

106 *a. Numerical model*

107 The ESCP comprises a number of channels varying significantly in width, from 60 m
108 upstream to 1000 m near the mouth, and thus a high resolution mesh is necessary to resolve the
109 many small channels in the domain. The numerical model used is the curvilinear-mesh, three-
110 dimensional Delft3D-Flow from Deltares (www.deltares.nl). This model is hydrostatic, and its

111 equations are solved by the method of finite differences (Delft Hydraulics, 2008). A curvilinear
112 mesh is appropriate for the domain, although there are some disadvantages in the horizontal
113 resolution distribution compared to unstructured meshes. Delft3D's curvilinear mesh is efficient in
114 minimizing noise due to the steps in the horizontal plane, and allows the mesh cells to follow the
115 channels more easily compared to non-curvilinear quadrangular meshes. The degree of non-
116 orthogonality between mesh elements is always smaller than 0.02 thus satisfying the criteria ($\cos \theta$
117 < 0.02), which helps to preserve numerical stability of the simulations (Delft Hydraulics, 2008).
118 The diagonal horizontal resolution ranges from ~20 m to ~300 m. The number of quadrangular
119 mesh cells on the horizontal plane is 22,928. A lower resolution is applied in the coastal region
120 ~[130-300] m, but this is increased toward the coast and the estuary ~[20-100] m (Figure 1B). The
121 refined mesh within the estuary combined with high water speeds requires the time-step to be
122 relatively small (around 1 second), to satisfy the Courant–Friedrichs–Lewy condition. The mesh
123 used in the simulations of the ESCP (Figure 1B) is relatively complex, covering a small part of the
124 Peruípe River, near the city of Nova Viçosa. This river is the main channel connecting the northern
125 and southern mouths. The main tributaries of the Caravelas River, namely the Cupído and Jaburuna
126 Rivers, are covered by the mesh. With 10 equally spaced sigma vertical layers, this mesh also
127 covers a few kilometers of the adjacent coastal region.

128 The bathymetry in the estuarine channels was obtained using an Echo sounder and Global
129 Position System. Two tide gauges were installed in Caravelas and Nova Viçosa (see locations A and
130 C in Figure 2), meant to remove the tides from the Echo sounder data. For the Peruípe River
131 estuary, the bathymetry was measured only in the first 6 km, near anchor station D. Thus an
132 extrapolation was applied, considering the depth to be 4 meters for the next 14 km along the Peruípe
133 River. The bathymetry was combined from these sources, and the triangular interpolation
134 application in Delft3D-Flow was used. The bottom topography has depths ranging from ~0.2 m to a
135 maximum of ~18 m (Tombo's Mouth), whilst in the coastal region do not exceed ~10 m.

136 A more detailed description of the field work carried out to obtain measurements of
 137 thermohaline properties and other parameters is provided in Appendix 2.

138
 139 *b. Model Boundary conditions, initial conditions and physical parameters*

140 Rainfall and river discharge measurements in the Peruípe River are shown in Figure 3B. The
 141 river discharge data, obtained from the National Agency of Waters ANA (<http://www.ana.gov.br/>),
 142 was measured at a gauge station upstream of the river, at station Helvécia n° 55510000 (code
 143 1739006). This station covers a large part of the drainage basin of the river. During rainy conditions
 144 the total drainage basin of the river may be used to estimate the total river flow to be applied at the
 145 upstream inflow boundary of the river. The factor to account for the missing drainage basin area is
 146 $\alpha = \frac{A_1 + A_2}{A_1} = 1.6$, in which station Helvécia $A_1 \sim 2,840 \text{ km}^2$, and the downstream area not covered
 147 by this gauge station is $A_2 \approx 1,760 \text{ km}^2$. The area values were obtained from the ANA
 148 (<http://hidroweb.ana.gov.br/>).

149 Data from the gauge station were also used to estimate the river discharge range for the
 150 Cupído and Jaburuna rivers. This was done by comparing their watershed areas with the watershed
 151 of the Peruípe river, and assuming homogeneous rainfall and evapotranspiration distributions over
 152 these areas (Andutta, 2011; Pereira et al., 2010). The total river flow into Caravelas Estuary was
 153 then roughly estimated using $Q = Q_P \beta$, where $\beta = 600/4600$ is the ratio between the catchment
 154 areas of the Caravelas (600 km^2) and the Peruípe ($A_1 + A_2 = 4600 \text{ km}^2$) rivers, and Q_P is the
 155 average discharge for the Peruípe). This estimation was adjusted by comparing observed flow
 156 velocities at locations A and B with model predictions.

157 The monthly estimate of fresh water inflow for the Peruípe River reveals small inflow for
 158 the dry season, often between June and September (see Figure 3C). The combined freshwater input
 159 from the Jaburuna and Cupído rivers estimated using the factor β is less than 10% of the river
 160 discharge into the Peruípe River. Because the field work was conducted during a relatively dry wet

161 season, when rainfall was negligible prior to and during measurements obtained in January 2008
162 (Figure 3A), it is logical not to consider the application of the factor α at the Helvécia gauge
163 station. Although this approach of river flow estimation is not required, the technique described
164 above would be required under homogeneous rainfall conditions over the drainage basin of the
165 Peruípe, Jaburuna and Cupído rivers.

166 The best fit between observations and model results was obtained using the mean river
167 discharge shown in Table 1 for the Cupído and Jaburuna rivers, and the daily measurements shown
168 in Figure 3B for the Peruípe River. In other words, the value measured at Helvécia gauge station
169 was used in the simulation with additional tuning to extrapolate results for the other two smaller
170 rivers.

171 .
172 **Preferred position for figure 3**
173
174

175
176 **Preferred position for Table 1**
177

178 The measurements from this tide gauge were compared with the simulation results during
179 neap and spring tides using the “Skill” method described below. In addition, a qualitative
180 comparison was carried out between the axial salinity distribution found in the simulations, and the
181 observed distribution presented in Schettini and Miranda (2010).

182 We used the initial condition of a homogeneous thermohaline distribution for the salinity (30
183 practical salinity unit - psu) and temperature (27 °C). The spin up simulation was made for about
184 two months to obtain a dynamic equilibrium condition. Since the temperature has previously been
185 found to be nearly homogeneous in this estuary (Andutta, 2011), its mean value was used for all
186 simulations. The first flow field and salinity distribution, obtained from the equilibrium condition,

187 was used to provide a varied initial field for simulations starting at slack waters in both spring and
 188 neap tidal conditions.

189 Computational modellers often assume that vertical eddy diffusion and viscosity coefficients
 190 vary in time, by using turbulent closure models, e.g. algebraic, *k-L*, *k-Epsilon* schemes. On the other
 191 hand, the horizontal eddy diffusivity, K_h , and horizontal viscosity coefficients, K_v , are often
 192 estimated according to the mesh element size (Okubo, 1971). Therefore, modellers need to choose a
 193 parameterisation scheme that provides the right amount of mixing in the estuary. We have
 194 considered the parameterisation of horizontal eddy viscosity by Uittenbogaard et al. (1992), which
 195 is available in Delft3D-Flow and reproduces well the turbulent fluxes of momentum.

196 The best fit between results and simulations was obtained assuming the horizontal eddy
 197 diffusivity, K_h , to be in the range of $\sim[2-30] \text{ m}^2 \text{ s}^{-1}$ with small and large values applied respectively
 198 to small and large mesh cells. The sensitivity analysis for K_h , was conducted following Okubo
 199 (1971). Because Okubo's formula applies for open-water, it was observed that it was not properly
 200 simulating the true dispersion in the estuary, thus a factor f was used to increase and decrease
 201 mixing at the sub-grid scale (See Equation 2). Varying f allowed us to achieve the best fit between
 202 measurements and model results.

$$203 \quad K_h = f [2.05 \times 10^{-4} \times d^{1.15}] \quad (2)$$

204
 205 where d is the mesh cell size (from ~ 20 to ~ 300 metres), and f is the factor set to different values
 206 but only shown for 2, 100, 150, 200, 250, 400 and 2000 in the sensitivity analyses (see Table 3).

207 The *k-Epsilon* turbulent closure scheme was used to compute values for the vertical viscosity
 208 and diffusivity. We assumed the typical Manning roughness coefficient of $(0.02 \text{ m}^{-1/3} \text{ s})$, which
 209 characterises the higher percentage of local sediment (Souza et al., 2013). This resulted in a Chézy
 210 coefficient of $\sim 40 \text{ m}^{-1/2}/\text{s}$. Wind speed and directions, assumed to be constant over this small region,
 211 were obtained at the Caravelas station from the Instituto Nacional de Meteorologia INMET (code
 212 INMET 86764), at (source: <http://www.inmet.gov.br/portal/>), see Figure 4.

Preferred position for figure 4

213
214

215 The wind was assumed to only affect mesh cells in coastal areas. In other words, the wind
216 stress did not affect mesh cells inside the estuarine channels. Moreover, Andutta et al. (2013)
217 applied Hansen and Rattray's analytical equation of the velocity and salinity components, and
218 demonstrated that the wind effect in January 2008 was negligible at station C (near Nova Viçosa
219 estuarine mouth), which is the closest to the coast. Hansen and Rattray's analytical solution required
220 an adjustment of no more than 0.02 Pascal for the wind stress, which correspond to wind speeds of
221 $\sim 3 \text{ m s}^{-1}$ (Andutta et al., 2013). South-southwestward alongshore currents occur between October
222 and January, while north-northeastward alongshore currents are observed during the fall and winter
223 months Lessa and Cirano (2006).

224 Sea level data from TOPEX were used to force tides at the open boundary nodes. A time
225 series of water surface elevation from May to July 2007 was recorded at Terminal Aracruz (TA in
226 Figure 2), which is a few kilometers away from the coastal open boundary. At TA a total of
227 16,264 tidal measurements were recorded at five minute intervals, and were processed using the
228 tidal component extraction program PACMARÉ (Franco, 2000). These tidal measurements were
229 used to obtain the amplitude and phase of the main tidal components, shown in Table 2.
230 Additionally, sea-level data were recorded at stations A and C from 14th to 19th of January 2008,
231 and these data were used to validate modelled sea-level oscillation (comparison shown in Results
232 and Discussion section). Sea surface elevation observations from sites A and C showed the same
233 phase, strongly suggesting that tides propagate across the shelf, because tides propagating along the
234 coast would results in a phase shift between sea level observations at sites A and C (see Figure 2).
235 The measurements of tidal heights of $\sim 1 \text{ m}$ and $\sim 3 \text{ m}$ during neap and spring tides, respectively.
236 This ranks as meso-tidal, according to the criteria of Davies (1964) for tidal classification. From
237 the tidal heights shown in Table 3, the tidal form-number is $[N_f = (K_1 + O_1) / (M_2 + S_2) =$
238 $0.19]$, indicating a semidiurnal tidal estuary (Defant, 1960). The tidal components from Table 2
239 represent over 97% of sea level variations for the estuarine system (Andutta, 2011).

Preferred position for Table 2

240
241
242
243
244
245

d. Model validation criteria

In order to quantify the agreement between the simulated velocity and salinity profiles the method suggested by Wilmott (1981), based on the Skill parameter was used. Accordingly, the skill is measured as follows

$$Skill = 1 - \frac{\sum |X_{mod} - X_{obs}|^2}{\sum \left(|X_{mod} - \bar{X}_{obs}| + |X_{obs} - \bar{X}_{obs}| \right)^2}, \quad (3)$$

247 where X_{obs} and X_{model} denote the observational and simulated properties, respectively, \bar{X}_{obs} being
248 the mean observational values. The Skill parameter varies from 1 to zero, with 1 indicating the best
249 fit, and zero indicating a complete disagreement between observation and model results.

250
251

e. Modelling approach to calculate the Transport Timescales

252 To quantify the residence time and exposure time 35 thousand numerical particles were
253 released in the estuary by coupling D-Waq PART with results from the Delft3D-FLOW (i.e. within
254 the subdomain denoted ω). Numerical particles were deployed near the bottom and top layers. The
255 particle concentration using conservative tracer module was normalized to value 1 within the
256 volume of ω . Therefore, the number of particles decreases when particles exit ω , and increases
257 when particles re-enter ω . The minimal initial number of particles, i.e. 25 thousand, was computed
258 considering a minimum thickness of 2 m and a grid cell of ~20 by 10 meters.

259 A total of four simulation scenarios were made: (S_1) particle released at high water in neap
260 tide, (S_2) particle released at low water in neap tide, (S_3) particle released at high water in spring
261 tide, and (S_4) particle released at low water in spring tide.

262 In order to be consistent with CART timescales, for the computation of the residence time,
263 particles are discarded once they have reached an open boundary, e.g. estuarine head or an open

264 boundary in coastal waters (de Brauwere et al., 2011; de Brye et al., 2012). The arithmetic mean of
 265 the individual residence times, φ , was computed as the time necessary for particles to exit the
 266 domain (ω) for the first time. As for the exposure time, the particles are assumed to immediately
 267 bounce back into the domain only at estuarine heads. This simplifying hypothesis is unlikely to
 268 entail any major error, since a particle crossing the upstream estuarine boundary in the upstream
 269 direction (because of diffusive processes) will most likely return into the estuary after a relatively
 270 small time under the influence of the river flow, e.g., the St. Johans River in Florida, which
 271 experiences backflows over significant durations (Hendrickson et al., 2003).

272 Results from residence and exposure times were used to estimate the return coefficient
 273 distribution. The residence and exposure times may vary according to the time of release, such as
 274 during neap/spring tides or high/low tides, and this would also affect the return coefficient. This
 275 notwithstanding, results of exposure and residence times must be calculated for the same conditions
 276 when computing the return coefficient, i.e. $r = (\Theta - \varphi) / \Theta$.

277

278 *f. The modified LOICZ analytical model*

279 The modified LOICZ model of Andutta et al. (2014) applies the salinity balance proposed
 280 by Fischer et al. (1979) into the original formulation of the LOICZ. This water renewal timescale
 281 model has been shown to be sensitive to changes to some of its free parameters (e.g. river flow and
 282 salinity gradient). We expect that the estimates of the timescales from our numerical results would
 283 fit within the ranges derived from the LOICZ model. Details of its derivation are provided in
 284 Andutta et al. (2014); however we provide the simplified relation for water renewal timescale.

285

$$286 \quad \frac{1}{T_p} = \frac{1}{T_1} + \frac{1}{T_2}, \quad (4)$$

287

288 where $T_1 = L/U$ and $T_2 = L^2 / K$ are the advective and dispersive timescales, respectively. L , U , K
 289 and T_p are respectively the selected estuarine segment length, the flow speed, the characteristic
 290 value of the longitudinal diffusivity and the water renewal timescale. This expression may be re-

291 written in terms of the dimensionless Péclet number $Pe = ULK^{-1}$, the ratio $P_e = T_2/T_1$ of the
 292 dispersive to the advective timescale. Similarly, this number provides a comparison of contributions
 293 from advective and dispersive processes to transport timescales, yielding

294

$$295 \quad T_P = \frac{VP_e}{Q_R(1+P_e)}. \quad (5)$$

296 Where V and Q_R denote the estuarine volume and river discharge, respectively. The contribution of
 297 advection to the total water renewal timescale T_P , θ ($0 \leq \theta \leq 1$), is given by

$$298 \quad \theta = T_P/T_1 = Q_R/(Q_R + Q_D), \quad (6)$$

299

300

301

302

303

304

305

306

307

308

309

310

311

312

313

314

315

316

317

318

319

320

321

322

323

324

325

326

327

328

329

330

331

332

333

334

335

336

337

where Q_D is the discharge. Equations (4) and (6) were used to generate the advective-dispersive
 diagram (shown later), whose results will be compared to the numerical results.

305 *g. The CART analytical model*

306 As previously mentioned, in the framework of CART, the TTS that may be used to calculate
 307 water renewal rates can be obtained at any time and position as the solution of partial differential
 308 equations (Deleersnijder et al., 2006; de Brye et al., 2012; Andutta et al., 2014). For instance,
 309 residence time and exposure time were estimated using calibrated/validated numerical simulations
 310 for the Scheldt Estuary (de Brauwere et al. 2011, de Brye et al. 2012). As an easy acceptable
 311 method, analytical solutions may provide results that are representative of real situations (e.g.
 312 CART and LOICZ). The idealised CART timescales were used to obtain the exact analytical
 313 solution of the so called return coefficient for the ESCP. Different values of the Péclet number were
 314 considered, in order to assess the axial variation of return coefficient values. The advective
 315 timescale, $T_1 = V/Q_R$, and a dispersive timescale, $T_2 = P_EV/Q_R$, are defined taking into consideration
 316 the estuarine volume V . Andutta et al. (2014) provides a detailed description depicting an idealized
 317 channel for the time scales.

318 Consider an estuarine channel ($-\infty < x < \infty$) with a constant cross-sectional area A , and a
 319 flow under steady-state. The volumetric flow rate is denoted as Q_R . The downstream and upstream
 320 boundaries of our idealised estuary are located at $x = L_0$ and $x = L_1$, respectively. The estuarine
 321 length is $L = L_0 - L_1$, and thus the volume is $V = AL$. The water velocity is then
 322 $U = Q_R / A = LQ_R / V$. For the abovementioned conditions, the residence time satisfies the adjoint
 323 of the classical passive tracer transport equation (Delhez et al. 2004, Andutta et al. 2014), i.e.

324

$$325 \quad \frac{d}{dx} \left(AK \frac{d\varphi}{dx} + Q_R \varphi \right) = -A \quad (7)$$

326

327 where, x , denotes the particle position. The solution for the equation needs to satisfy the upstream
 328 and downstream boundary conditions,

329

$$330 \quad \varphi(L_1) = 0 = \varphi(L_0). \quad (8)$$

331

332 It represents the average time required by particles initially located in the interval $[x, x + \delta x]$
 333 (with $\delta x \rightarrow 0$) to reach one of the open boundaries. The solution is then easily derived:

334

$$335 \quad \varphi(x) = \frac{V}{Q_R} \left(1 - \frac{\xi}{L} \right) + \frac{V}{Q_R} \left(\frac{e^{-Pe} - e^{-Pe \xi/L}}{1 - e^{-Pe}} \right) \quad (9)$$

336 where $\xi = x - L_1$.

337 The exposure time was also derived (Andutta et al., 2014), and is defined in the domain of interest
 338 and its surrounding environment.

$$339 \quad -\infty \leq x \leq L_1 \quad : \quad \Theta(x) = \frac{V}{Q_R} \quad (10a)$$

$$340 \quad L_1 \leq x \leq L_0 \quad : \quad \Theta(x) = \frac{V}{Q_R} \left(1 - \frac{\xi}{L} \right) + \frac{V}{Q_R} \left(\frac{1 - e^{-Pe \xi/L}}{Pe} \right) \quad (10b)$$

$$341 \quad L_0 \leq x < \infty \quad : \quad \Theta(x) = \frac{V}{Q_R} \left(\frac{e^{-Pe} - 1}{Pe} e^{-Pe \xi/L} \right) \quad (10c)$$

342

343 From Equations (9) and (10), which are valid within the upstream and downstream open
 344 boundaries, the return coefficient is:

345

$$346 \quad r = \frac{\Theta(x) - \varphi(x)}{\Theta(x)} = \frac{\left(\frac{1 - e^{-Pe \zeta/L}}{Pe} \right) - \left(\frac{e^{-Pe} - e^{-Pe \zeta/L}}{1 - e^{-Pe}} \right)}{\left(1 - \frac{\zeta}{L} \right) + \left(\frac{1 - e^{-Pe \zeta/L}}{Pe} \right)} \quad (11)$$

347 Note that r is bounded by $[0,1]$, as mentioned before.

348 In principle, the residence time and the exposure time can be obtained by solving classical
 349 passive transport equations. However, to do so, time- and position-dependent concentrations must
 350 first be obtained and, then, time and space integral must be performed to derive the relevant
 351 timescales. This is not straightforward, even for highly idealised flows. This is why it is preferable
 352 to have recourse to the adjoint method established by Delhez et al. (2004), which requires the
 353 solution of simpler differential problems to be determined: in the present case, only ordinary
 354 differential equations are to be dealt with rather than partial differential ones. The disadvantage of
 355 this approach is that the theoretical underpinning of an adjoint model sometimes appears elusive,
 356 which is probably the reason why Errico (1997) wrote a general, enlightening paper on this matter,
 357 explaining the nature and purpose of adjoint models.

358

359 3. Results and Discussion

360

361 *a. Model calibration of salinity, velocity and tides*

362 We carried out a sensitivity analysis considering different values for the horizontal diffusion
 363 coefficient k_h using Equation 2. These adjustments of factor f for the horizontal diffusivity based on
 364 the grid size allowed us to obtain a proper representation of the salinity field and its time variability.

365

Preferred position for Table 3

366 The mean Skill parameters for the simulation are shown in Table 3 for different values of
367 factor f , which was described with Equation 2. The comparison of sea-level oscillation over a tidal
368 modulation period, from the 14th to the 29th of January 2008, showed good skill values for locations
369 A (Figure 5) and C (not shown), and the Skill parameter for tides was calculated to be over 0.97 for
370 both locations, i.e. A and C. The comparison of tides, velocity, and salinity showed good skill
371 values during spring tides (not shown), and reasonable values during neap tides (Figure 6).

372
373
374
375

Preferred position for figure 5
Preferred position for figure 6

376 The Skill parameter for the water column height variation in time was calculated to be over
377 0.98 for all the sites under neap and spring tides (Table 4), and the tidal ranges were ~1.0 m and
378 ~2.5 m for neap and spring tides, respectively. Observations have shown that the tidal phase
379 between sites A (Caravelas mouth) and C (Peruípe mouth) is almost the same. The similarity of
380 their phases indicates that tides propagate mainly perpendicular to the coast line in this region, a
381 result which is in close agreement with observations previously reported by Lessa and
382 Cyrano (2006).

383 For the modeled velocity validation, good results (Skill from 0.77 to 0.93) were obtained in
384 spring tides in the estuaries of Caravelas (sites A and B) and Nova Viçosa (sites C and D). For neap
385 tides due to small differences on tidal asymmetry, the Skill was lower, at ~ 0.6.

386 The model agreed well with observations of maximum ebb and flood currents at site A. The
387 model also properly simulated the velocity profiles for sites B, C, and D. Therefore, the description
388 of maximum ebb and flood currents from in-situ data also apply to the model simulations. At site B
389 there were maximum speeds of ~0.5 m s⁻¹ and 1.0 m s⁻¹ (ebb events), and ~-0.3 m s⁻¹ and ~-0.6 m s⁻¹
390 (flood events), during neap and spring tides, respectively. For site A the vertical shear of the
391 velocity was negligible in flood and ebb conditions, while for site B there was a small vertical shear
392 of the horizontal velocity during ebb events. During flood events, the water velocity was
393 homogenous over the water column. In addition, a residual velocity of ~0.05 m s⁻¹ was calculated at

394 site B, indicating a residual circulation from Nova Viçosa towards the Caravelas River. Site A had a
395 residual current of $\sim 0.06 \text{ m s}^{-1}$, indicating a small discharge from the Cupído and Jaburuna Rivers.
396 At sites C and D, located in the Peruípe River, the downstream velocities showed more intensity
397 than observed in the Caravelas Channel. For site C the downstream velocities varied from $\sim -0.9 \text{ m}$
398 s^{-1} to $\sim -1.5 \text{ m s}^{-1}$, for neap and spring tides, respectively. During flood events, the velocities were \sim
399 0.3 m s^{-1} and $\sim -0.7 \text{ m s}^{-1}$, for neap and spring tides, respectively. At site D the maximum
400 downstream velocities were only $\sim 0.7 \text{ m s}^{-1}$ and $\sim 1.0 \text{ m s}^{-1}$ at neap and spring tides, and upstream
401 velocities were $\sim -0.3 \text{ m s}^{-1}$ and $\sim -0.4 \text{ m s}^{-1}$. The residual velocities at sites C and D, which have
402 values of $\sim 0.10 \text{ m s}^{-1}$ to $\sim 0.15 \text{ m s}^{-1}$, indicate a higher advective contribution from the Peruípe River
403 compared with the Caravelas estuary.

404 In addition to the tides and the velocity field, the model simulated the temporal variation of
405 the salinity well for all sites (A, B, C, and D). During spring tides the calculated Skill values were
406 over 0.83, while for neap tides they were over 0.73 (Table 4). At the Caravelas estuarine channel,
407 $\sim 3 \text{ km}$ near the mouth (site A), during low tide, salinity was observed in intervals of $\sim 34.5 \text{ psu}$ to
408 $\sim 35.0 \text{ psu}$ and $\sim 34.0 \text{ psu}$ to $\sim 34.5 \text{ psu}$ for the observational and theoretical results,
409 respectively. About 6 km away from the mouth we obtained a good agreement for the salinity, with
410 $\sim 32.0 \text{ psu}$ and $\sim 32.5 \text{ psu}$ for observation and simulation, respectively. In the vicinity of the
411 interconnection with Cupído and Jaburuna Rivers (site B), which is about 12 km upstream from the
412 mouth, the salinity decreased to $\sim 30.0 \text{ psu}$ and $\sim 28.5 \text{ psu}$ for the observational and calculated
413 results, respectively. At high tide, near the mouth (site A) and at a distance of 6 km from the mouth,
414 the salinity was $\sim 36.5 \text{ psu}$ and $\sim 36.0 \text{ psu}$, respectively, for both simulation and field measurements.
415 In the upper reaches of the estuary, near the junction of the rivers, Cupído and Jaburuna ($\sim 12 \text{ km}$
416 from the mouth), a close agreement between simulated and observed salinity values ($\sim 33.0 \text{ psu}$) was
417 obtained at high tide. Along the Peruípe River estuary at neap tides, the surface salinities vary in the
418 range of 20.0 psu to 34.0 psu at the surface, and 32.5 psu to 36.0 psu near the bottom. The region of
419 Nova Viçosa has more vertical stratification of the salinity than at sites A and B in the Caravelas

420 River. This is due to Peruípe River's larger freshwater discharge. The observed value of ~36.0 psu
421 near the bottom is characteristic of the Tropical Water Mass, which was already reported to enter
422 this estuarine system (Schettini et al., 2010). During spring tides the vertical mixing causes the
423 erosion of the halocline, and thus decreases vertical stratification. This results in a smaller vertical
424 variation of 31.0 psu to 36.0 psu from the surface to the bottom.

425 **Preferred position for Table 4**

426 A comparison of the axial distribution of salinity was made for the Caravelas River (Figure
427 7A,B). For the first 12 km along the estuarine channel, results from simulations were compared to
428 observations made by Schettini and Miranda (2010). The measurements were obtained on the 10th
429 of April, 2001 during spring tides. Although the field data are likely to be from different conditions
430 of river flow, the simulation showed a good correlation of the axial distribution of the salinity in the
431 Caravelas River (See Figures 7C and 7D), with values of $R^2 \sim 0.97$ and $R^2 \sim 0.99$ for low and high
432 tides respectively. This indicates that the model has well represented the mixing processes in the
433 Caravelas Estuary. During low tide (Figure 7A,C), a good agreement is found near the mouth, with
434 salinity values of ~35.2 psu and ~ 34.5 psu, for the model results and observations, respectively. At
435 nearly 6 km upstream, there is still a good agreement ($R^2 \sim 0.99$) with the salinity values of ~33
436 psu (model), and ~32 psu (observation). Further upstream and near the inter-connection between the
437 Cupído and Jaburuna rivers (i.e. ~ 12 km upstream), the agreement is slightly poorer with the
438 salinity values of ~30 psu (model) and ~29 psu (observation). At high tide (Figure 7B, D), the
439 model predicted the longitudinal salinity variations well along the Caravelas Channel. The salinity
440 values near the mouth were ~36.4 psu (model and observation), and reduced to ~36 psu 6 km
441 further upstream. Moreover, during high tides the agreement was also good near the channel
442 between the Cupído and Jaburuna rivers with salinity of ~33 psu.

443 **Preferred position for figure 7**

444
445 *b. Results of the residence time, the exposure time and the return coefficient*

446

447 The transport timescales, namely residence time (φ), exposure time (Θ), and the return
448 coefficient (r), were estimated for the Caravelas and Peruípe estuarine channels with simulation
449 under different scenarios, i.e. S₁ to S₄ (Figures 8, and 9).

450 For scenarios S₁ and S₃ (Figure 8), the residence time along the Caravelas Channel, from the
451 mouth to 12 km upstream, was found to vary from 0 to ~15.0 days. The inflow boundaries of the
452 Cupído and Jaburuna rivers were found to have residence times of ~27 and ~22 days, respectively.
453 For the Peruípe Channel the residence times ranged from 0 to ~7.4 days, from the mouth to 5 km
454 upstream, with a maximum value of ~18 days at the inflow boundary of the Peruípe Estuary.

455 The residence time estimated at ~6 km further upstream in the Caravelas Estuary ($\varphi = 11.7$
456 days) is almost three times larger than the residence time calculated for the same distance along the
457 Peruípe Estuary ($\varphi < 4.4$ days). The difference between results in the Caravelas and the Peruípe
458 estuaries is due to the larger velocity contribution in the Peruípe Estuary.

459 Comparing scenarios S₁ and S₃, the residence time was found to be slightly lower for S₃ (c.a.
460 a few hours) and this difference is due to increased diffusive contribution during stronger spring
461 tidal conditions. In contrast to scenarios S₁ and S₃, the simulations considering scenarios S₂ and S₄
462 yielded an increased residence time. This increase was maximum near the estuarine mouths (~5
463 days), and observed to reduce in the upstream direction (few hours). The increase in residence time
464 for particles released in slack water of low tide is caused by tidal excursion from reversing currents
465 (i.e. flood currents). These results reflect and add value to recent simulations by de Brye et al.
466 (2012) for the Scheldt Estuary (in Belgium and the Netherlands), whose results showed larger
467 residence time values for particles released at slack water of low tides than for high tides (difference
468 of a few days).

469 The virtual Lagrangian particles showed that a negligible number of particles crossed the
470 connecting channel between the Caravelas (ω_1) and Peruípe Estuaries (ω_2), which indicates that this
471 relatively narrow and shallow interconnection channel allows little exchange of water properties
472 between these estuaries. Moreover, the residence time is observed to be larger within the

473 enlargement of the interconnecting channel between these two estuaries. Schettini and Miranda
 474 (2010) and Schettini et al. (2013) have addressed the importance of the interconnection channel
 475 between Caravelas and Peruípe, and found that sediment deposited near the Caravelas mouth was
 476 both inner shelf local resuspension and upstream transport, or sourced from the Peruípe River via
 477 the interconnection channel.

478
 479
 480

Preferred position for figure 8

481 Exposure time results showed that particles re-entered the system for up to two days (Figure
 482 9). Note that the difference between the exposure time and the residence time ($\Theta - \varphi$) showed little
 483 spatial variation for scenarios S_1 and S_3 .

484
 485

Preferred position for figure 9

486 The spatially averaged difference between exposure and residence times ($\Theta - \varphi$) are
 487 calculated in days, and its respective RMSE to be $\sim 1.98 \pm 0.06$ for S_1 , $\sim 1.87 \pm 0.12$ for S_2 , ~ 1.92
 488 ± 0.07 for S_3 , $\sim 2.19 \pm 0.08$ for S_4 . These results strongly suggest that ($\Theta - \varphi \sim \text{const.}$) for the
 489 ESCP under the four different scenarios considered. The results also suggest that $t_3 - t_2$ varies little
 490 away from the open boundaries, so particles deployed at different times and locations in the estuary
 491 re-enter for similar lengths of time, assuming the circulation in coastal waters does not considerably
 492 change over time due to additional forcings, e.g. sudden alongshore wind driven currents.

493 Equation (5) was used to estimate the range of water renewal timescales for the Caravelas
 494 and Peruípe estuaries using the parameters given in the appendices of Andutta et al. (2014), see
 495 Figure 10. The straight line labelled θ (lowercase) indicate the relative advective contribution to
 496 water renewal, where $0 \leq \theta \leq 1$. The line at $\theta = 0.5$ separates the areas where transport is
 497 dominated by advection (diagram upper zone, $\theta > 0.5$) and dispersion (diagram lower zone, $\theta <$
 498 0.5).

499 The Caravelas and Peruípe estuaries have mean depths of ~ 6.5 and ~ 7.5 meters,
 500 respectively, and the maximum and minimum tidal ranges in these estuaries are ~ 2.5 and ~ 0.5

501 meters. According to Andutta et al. (2013), these tidal ranges combined with the relatively the small
502 depths result in a high rate of change of the potential energy ($\sim 6.1 \text{ J m}^{-3} \text{ s}^{-1}$), which contributes
503 towards large dispersion. It is valid to compare these results to the Sheldt Estuary, where tidal
504 oscillation is typically 4-5 meters along the first ~ 100 km, and where the mean water depth is ~ 10
505 meters. Tidal range in the Sheldt can reach ~ 7 m, which is about 45% of the mean water depth
506 value for the first ~ 25 km near the estuarine mouth (Soertaert and Herman, 1995; de Brye et al.
507 2012), and this system is classified as well-mixed due to dispersion prevailing over advection. The
508 numerical results for the ESCP fit within the timescale ranges estimated using the simple LOICZ
509 method.

510
511
512

Preferred position for figure 10

513 The return coefficient cannot be calculated using the modified LOICZ model. However, it
514 was computed numerically and compared to the non-dimensional solution obtained using CART.
515 The return coefficient converges to one at the estuarine mouths and near estuarine heads (Figure 11,
516 for all scenarios S_1 to S_4 and Figure 12B). However, this is only a direct consequence of the
517 definition of the residence time, which converges to zero at the entrance, and thus the return
518 coefficient will always increase towards unity. r was observed to be smaller upstream, because the
519 ratio $(\Theta - \varphi)/\Theta$ is likely to decrease. It can be noticed that the axial variation of the return
520 coefficient is similar for both CART solution and numerical approach (Figures 11 and 12C). The
521 return coefficient calculated from CART and from numerical simulations is observed to increase
522 towards the upstream boundary. This increase towards the estuarine head is due to the boundary
523 condition assumed in the analytical and numerical solutions, where particles do not re-enter the
524 domain after crossing the estuarine head, although in a real estuary water particles would re-enter
525 through the estuarine head due to river flow conditions.

526 Figure 12A shows results of the residence and exposure time and return coefficient for a
527 range of values of the Péclet number. High values of the Péclet number yield a boundary layer in
528 the vicinity of the upstream location.

529 The greater the relative importance of advection, the less likely it is that dispersion will
530 cause a water particle to hit the upstream boundary of the domain ($x = L_0$). In accordance with their
531 definitions, the exposure time is larger than the residence time for any location in the domain ($L_1 \leq$
532 $\xi/L \leq L_0$). These idealised results of the return coefficient were used to access results obtained
533 from our numerical simulations.

534

535
536 **Preferred position for figure 11**
537

538 **Preferred position for figure 12**
539

540 In the illustration shown in Figure 11A, the ratio is simply the difference between times t_3
541 and t_2 . Evidently this is a simple case where the particle is assumed to have re-entered the domain
542 only once.

543 Particles are expected to first cross the estuarine mouth during ebb currents, which would be
544 alternating with flood currents and dispersive processes. Therefore, we could presume that
545 Lagrangian particles would have a time window of ~ 6.5 hours to cross the entrance (for semi-
546 diurnal tidal estuaries), and this time window would then close for ~ 6.5 hours (the period of flood
547 currents).

548 Our simulations were for relatively calm weather conditions, which were predominant over
549 the region, c.a. wind speeds in the range $1-4 \text{ m s}^{-1}$ (wind from NE). Andutta et al. (2013) showed
550 that wind conditions did not affect the water circulation in this estuarine system in January 2008.
551 However, for stronger wind conditions the results would not be the same. Evidently alongshore
552 wind-driven currents would reduce the difference between the exposure time and the residence
553 time, and the return coefficient would thus decrease towards zero. This is because alongshore
554 currents inhibit the propensity of particles to re-enter the estuarine system. The alongshore shelf
555 currents are observed to be driven by the N-S migration of the South Atlantic High between
556 summer and winter. South-southwestward alongshore currents occur between October and January,
557 while stronger north-northeastward alongshore currents are observed during the fall and winter
558 months (Lessa and Cirano, 2006).

559

560 **4. Conclusions**

561

562 *Overall goal*

563 This study provides the first estimates of the residence time, exposure time and the return
564 coefficient for the Caravelas and Peruípe estuaries and might be a reference for future studies
565 related to the control of pollutants and sediment transport. These transport timescales were
566 estimated using a Lagrangian model only as a tool, and this model has been properly calibrated and
567 validated using field data.

568 *Specific conclusions*

569 • *Achievements regarding goals (1 and 2)*

570 The residence time for particles released far upstream in the Caravelas Estuary was found to
571 be nearly 3 weeks for particles, regardless of whether they are released at high or low tide, and is
572 driven by tidal dispersion combined with the discharge from the Cupído and Jaburuna Rivers
573 (typical range of 4 to 9 m³ s⁻¹). These results are consistent with previous estimates derived from
574 simple analytical solutions (Andutta et al., 2014), see Figure 10. For the Peruípe Estuary, our
575 estimates of the residence time were for less than one week, due to the tidal dispersion combined
576 with the larger river input from the Peruípe River (typical range of 20 to 70 m³ s⁻¹).

577 The transport timescales (exposure and residence times) were found to be quite similar for
578 particles released in high tide under spring and neap tidal conditions, thus confirming previous
579 estimations made for the Scheldt Estuary (de Brye et al., 2012). In contrast, the transport timescales
580 were shown to be more sensitive to tidal-phase release time (i.e. high or low tides) in this estuarine
581 system. Similar observations were made for the Scheldt Estuary (de Brauwere et al., 2011), in
582 which there was a difference of days for results of residence time using particles released at high
583 and low tides. This suggests that tidal-phase release time for a meso-tidal shallow estuary forced by
584 low-moderate river discharge conditions is important for quantification of TTS, especially for water
585 particles near mouths where larger tidal excursions are expected compared to locations further
586 upstream, and since their initial movement would be upstream/downstream if released during
587 low/high tide, respectively.

588 The Lagrangian simulation also showed that the narrow and shallow inter-connecting
589 channel between the Peruípe and Caravelas estuaries allows little water exchange between the two
590 estuaries, and only a few particles were capable of crossing the inter-connection passage with
591 prevailing direction from the Peruípe to the Caravelas, in agreement with Schettini et al. (2013).
592 Therefore, both exposure time and residence time were large at that location, and the exchange of
593 water properties is likely to happen through alongshore currents at inner coastal areas.

594 • *Achievements regarding goal (3)*

595 Similarly to the exposure and residence times, the return coefficient was shown to be more
596 sensitive to tidal phase (high and low tide), than to neap and spring tidal conditions. It may be
597 summarized as follows: (1) the return coefficient is larger for particles released at high tide than at
598 low tide; (2) the return coefficient is larger for particles released during spring tides than during
599 neap tides.

600 For these two estuaries the exposure time was higher than the residence time in all
601 simulations, thus showing that water may return to the system after having first crossed the mouth.
602 The propensity of this water to return to the estuary was quantified using the return coefficient,
603 which depends on the difference between the exposure and residence times, and thus also on the
604 residual circulation due to river discharge, as well as the circulation in coastal waters. For instance,
605 swift longshore currents decrease the difference between the exposure and residence times, and
606 therefore reduce the return coefficient. The wind conditions over our measurement period were
607 characteristic of calm weather, c.a. a few m s^{-1} (see Figure 4), and different scenarios may produce
608 different results for the transport timescales, for instance under stronger north-northeastward
609 alongshore currents which are often observed during the fall and winter months Lessa and Cirano
610 (2006). Due to its definition, the return coefficient is predicted to be larger at the estuarine mouths,
611 because the residence time tends to zero (see Equation 1). Our results have additionally shown that
612 for our scenarios the difference between exposure and residence times ($\Theta - \varphi$) is nearly constant
613 within our domain. This can also be observed from our analytical solution (Figure 12C).

614

615 **6. Acknowledgements**

616

617 We acknowledge the Conselho Nacional de Desenvolvimento Científico e Tecnológico
618 (CNPq) grant 420219/2005-6 to Eurico Cabral de Oliveira, and the fellowships (Procs. LBM-
619 302069/2004-6, CAFS-306217/2007-4 and ES-308303/2006-7). We also acknowledge the
620 assistance in the field work from Carlos A. F. Schettini, Eduardo Siegle, Mario Pereira, Piero L. F.
621 Mazzini, Vitor M. Izumi, and the collaboration of other graduate students and technicians of the
622 Dept. of Physical, Chemistry and Geology of IO-USP, PPGGeo/UFRGS and UFRN. Eric
623 Deleersnijder is an honorary Research Associate with the Belgian Fund for Scientific Research
624 (F.R.S.-FNRS).

625

626 **References**

627

- 628 Andutta, F.P., Ridd, P.V., Deleersnijder, E., Prandle, D., 2014. Using field data for estimating
629 estuarine water transport timescales and the associated return coefficient. *Progress in*
630 *Oceanography* 120, 139–153, doi: 10.1016/j.pocean.2013.08.009.
- 631 Andutta, F.P., Miranda, L., Schettini, C.A.F., Siegle, E., da Silva, M.P., Izumi, V.M., Chagas, F.M.,
632 2013. Temporal variations of Temperature, Salinity and circulation in the Peruípe River
633 Estuary (Nova Viçosa, BA). *Continental Shelf Research* 70, 36–45, doi:
634 10.1016/j.csr.2013.03.013.
- 635 Andutta, F.P., 2011. The estuarine system of the Caravelas and Peruípe rivers (Bahia):
636 Observations, simulations, residence time, and advective and diffusive processes, PhD Thesis.
637 IO-USP, Oceanography Institute of the University of São Paulo, 121 pp.
- 638 Chaves, F.O., Soares, M.L.G., Estrada, G.C.D., Cavalcanti, V.F., 2009. Maintenance of mangrove
639 forest through the conservation of coastal ecosystems. *Journal of Coastal Research* 56, 395–
640 399.
- 641 Costa Jr., O.S., Leão, Z.M.A.N., Nimmo, M., Attrill, M.J., 2000. Nutrifcation impacts on coral
642 reefs from northern Bahia, Brazil. *Hydrobiologia* 440, 307–315, doi:
643 10.1023/A:1004104118208.

- 644 Defant, A., 1960. *Physical Oceanography*, Pergamon Press, New York 2, 598 pp.
- 645 Deleersnijder, E., Beckers, J.-M., Delhez, E.J.M., 2006, On the behaviour of the residence time at
646 the bottom of the mixed layer, *Environmental Fluid Mechanics* 6, 541–547.
- 647 Delft Hydraulics, 2008. *Delft-3D Flow Manual*, Delft Hydraulics, Delft, Holanda, 674 pp.
- 648 Delhez, E.J.M., Heemink, A.W., Deleersnijder, E., 2004. Residence time in a semi-enclosed domain
649 from the solution of an adjoint problem, *Estuarine, Coastal and Shelf Science* 61, 691–702.
- 650 Delhez, E.J.M., de Brye, B., de Brauwere, A., Deleersnijder, E., 2014. Residence time vs influence
651 time. *Journal of Marine System* 132, 185–195, doi: 10.1016/j.jmarsys.2013.12.005.
- 652 de Brauwere, A., de Brye, B., Blaise, S., Deleersnijder, E., 2011. Residence time, exposure time and
653 connectivity in the Scheldt Estuary. *Journal of Marine Systems* 84, 85–95, doi:
654 10.1016/j.jmarsys.2010.10.001.
- 655 de Brye B., de Brauwere, A., Gourgue, O., Delhez, E.J.M., Deleersnijder, E., 2012, Water renewal
656 timescales in the Scheldt Estuary, *Journal of Marine Systems* 94, 74–86.
- 657 Errico, R.M., 1997, What is an adjoint model?, *Bulletin of the American Meteorological Society*,
658 78, 2577-2591.
- 659 Fischer, H.B., List, E.Y., Koh, R.C.Y., Imberger, J., Brooks, N.H., 1979. *Mixing in Inland and*
660 *Coastal Waters*. Academic Press, New York, 483 pp.
- 661 Franco, A.S., 2000. *Mares: Programa para previsão e análise*. Manual, BSP, São Paulo, 36pp.
- 662 Gaeta, S.A., Lorenzetti, J.A., Miranda, L. B., Susini-Ribeiro, S.M.M., Pompeu, M., Araujo, C.E.S.,
663 1999. The Vitoria Eddy and its relation to the phytoplankton biomass and primary
664 productivity during the austral fall of 1995. *Brazilian Archive of Fishery and Marine Research*
665 47(2-3), 253–270.
- 666 Hendrickson, J.C., E.F. Lowe, D. Dobberfuhl, P. Sucsy, and D. Campbell. 2003. Characteristics of
667 Accelerated Eutrophication in the Lower St. Johns River Estuary and Recommended Targets
668 to Achieve Water Quality Goals for the Fulfillment TMDL and PLRG Objectives. Department
669 of Water Resources, St. Johns River Water Management District, Palatka, Florida.
- 670 Holzer, M., Hall, T.M., 2000. Transit-time and tracer-age distributions in geophysical flows.
671 *Journal of the Atmospheric Sciences* 57, 3539–3558.
- 672 Ketchum, B.H., 1951. The exchanges of fresh and salt water in tidal estuaries. *Journal of Marine*
673 *Research* 10, 18–38.
- 674 Knoppers, B., Ekau, W., Figueredo, A. G., 1999. The coast and shelf of east northeast Brazil and
675 material transport. *Geo-Marine Letters* 19, 171–178, doi: 10.1007/s003670050106.
- 676 Leipe, T., Knoppers, B., Marone, E., Camargo, R., 1999. Suspended matter transport in coral reef
677 waters of the Abrolhos bank Brazil. *Geo-Marine Letters* 19, 186–195, doi: 1
678 0.1007/s003670050108.

- 679 Lessa, G.C., Cirano, M., 2006. On the circulation of a coastal channel within the Abrolhos Coral-
680 Reef system-Southern Bahia, Brazilian Journal of Coastal Research 39, 450–453.
- 681 Monsen, N.E., Cloern, J.E., Lucas, L.V., Monismith, S.G., 2002. A Comment on the Use of
682 Flushing Time, Residence Time, and Age as Transport Time Scales, Limnology and
683 Oceanography 47, 1545–1553.
- 684 Okubo, A., 1971. Diffusion Diagrams, Deep-Sea Research 18, 789–802, doi: 10.1016/0011-
685 7471(71)90046-5.
- 686 Pereira, M.D., Siegle, E., Miranda, L.B., Schettini, C.A.F., 2010. Hidrodinâmica e transporte de
687 material particulado em suspensão sazonal em um estuário dominado por maré: estuário de
688 Caravelas (BA), Revista Brasileira de Geofísica 28(3), 427–444, doi: 10.1590/S0102-
689 261X2010000300008.
- 690 Schettini, C.A.F., Pereira, M.D., Siegle, E., Miranda, L.B., Silva, M.P., 2013. Residual fluxes of
691 suspended sediment in a tidally dominated tropical estuary. Continental Shelf Research 70
692 (SI), 27–35, doi: 10.1016/j.csr.2013.03.006.
- 693 Schettini, C.A.F., Miranda, L.B., 2010. Circulation and Suspended Matter Transport in a Tidally
694 Dominated Estuary: Caravelas Estuary, Bahia, Brazil. Revista Brasileira de Oceanografia 58,
695 1–11, doi: 10.1590/S1679-87592010000100001.
- 696 Sheldon, J.E., Alber M., 2006. The Calculation of Estuarine Turnover Times Using Freshwater
697 Fraction and Tidal Prism Models: A Critical Evaluation. Estuaries and Coasts 29, 133–146.
- 698 Smagorinsky, I., 1963. General circulation experiment with Primitive equations. Monthly Weather
699 Review 91, 91e164.
- 700 Summerhayes, C., Melo, U.D., Barreto, H., 1976. The influence of upwelling on suspended matter
701 and shelf sediments off southeastern Brazil, Journal of Sedimentary Petrology 46, 819–828.
- 702 Teixeira, C.E.P., 2006. Caracterização e variabilidade da hidrodinâmica da zona costeira adjacente
703 ao banco de Abrolhos, MSc Thesis. IO-USP, Oceanography Institute of the University of São
704 Paulo, 93 pp.
- 705 Uittenbogaard, R. E., J. A. T. M. van Kester and G. S. Stelling, 1992. Implementation of three
706 turbulence models in 3D-TRISULA for rectangular grids. Tech. Rep. Z81, WL j Delft
707 Hydraulics, Delft, The Netherlands.
- 708 Wilmott, C. J., 1981. On the validation of models, Physical Geography 2, 184–194.
- 709 Zimmerman, F., 1988. Estuarine residence times, in B. Kjerfve (Ed.), Hydrodynamics of estuaries,
710 vol. 1, pp. 75–84, CRC Press.

711

712

Figure 2

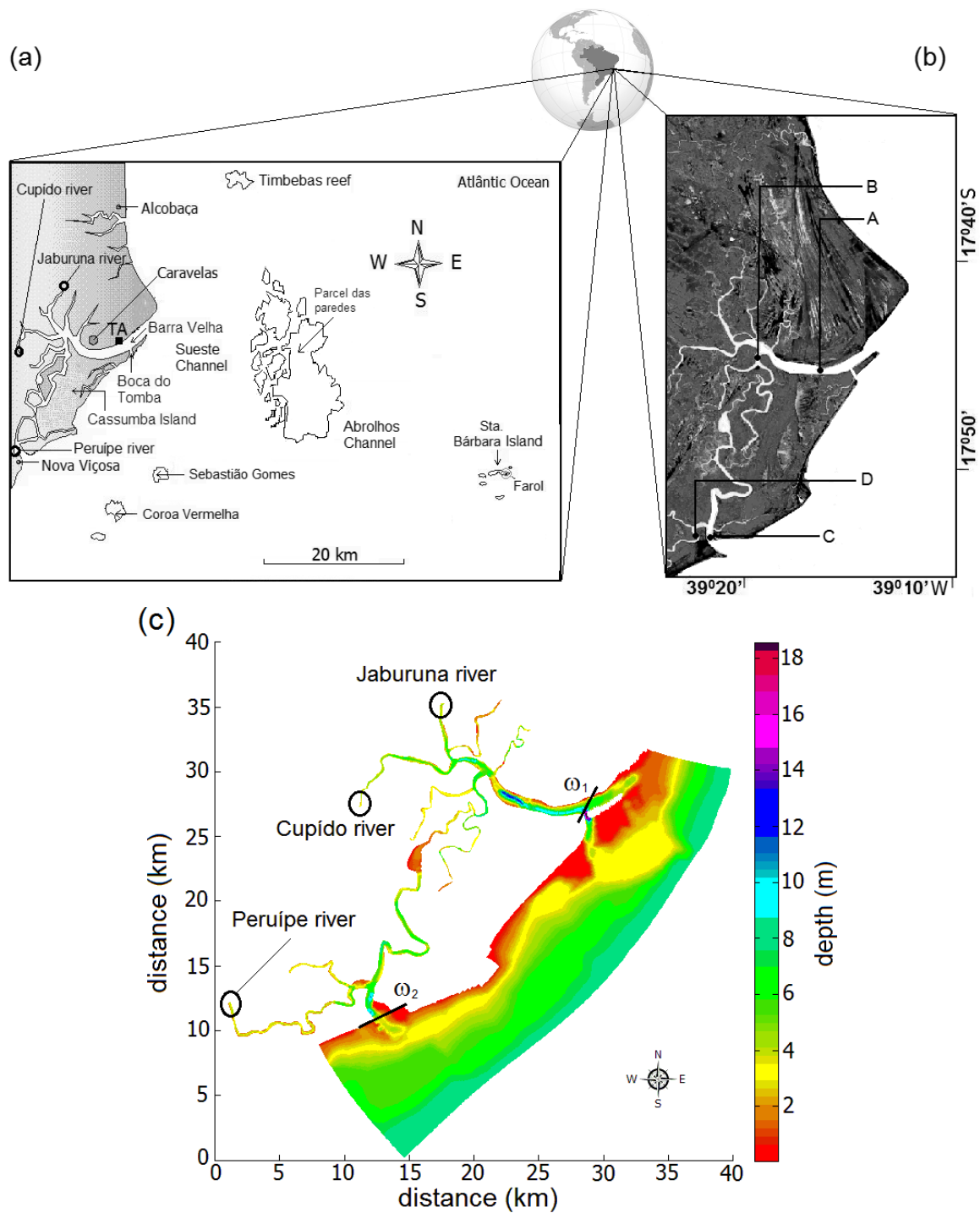


Figure 2 – (a) Geographic location of the estuarine system comprising the Caravelas and Peruípe rivers. Aracruz terminal harbour – TA, and the Sueste and Abrolhos channels, the Parcel das paredes and the National Marine Park of Abrolhos. (b) Detailed image of the estuarine system, and location of the oceanographic mooring sites A and B in Caravelas area, and C and D in Nova Viçosa area, where D is referred as site E at Andutta et al., 2013b. (c) numerical domain with ω_1 and ω_2 denoting the limit of the control domain ω to compute the transport timescales.

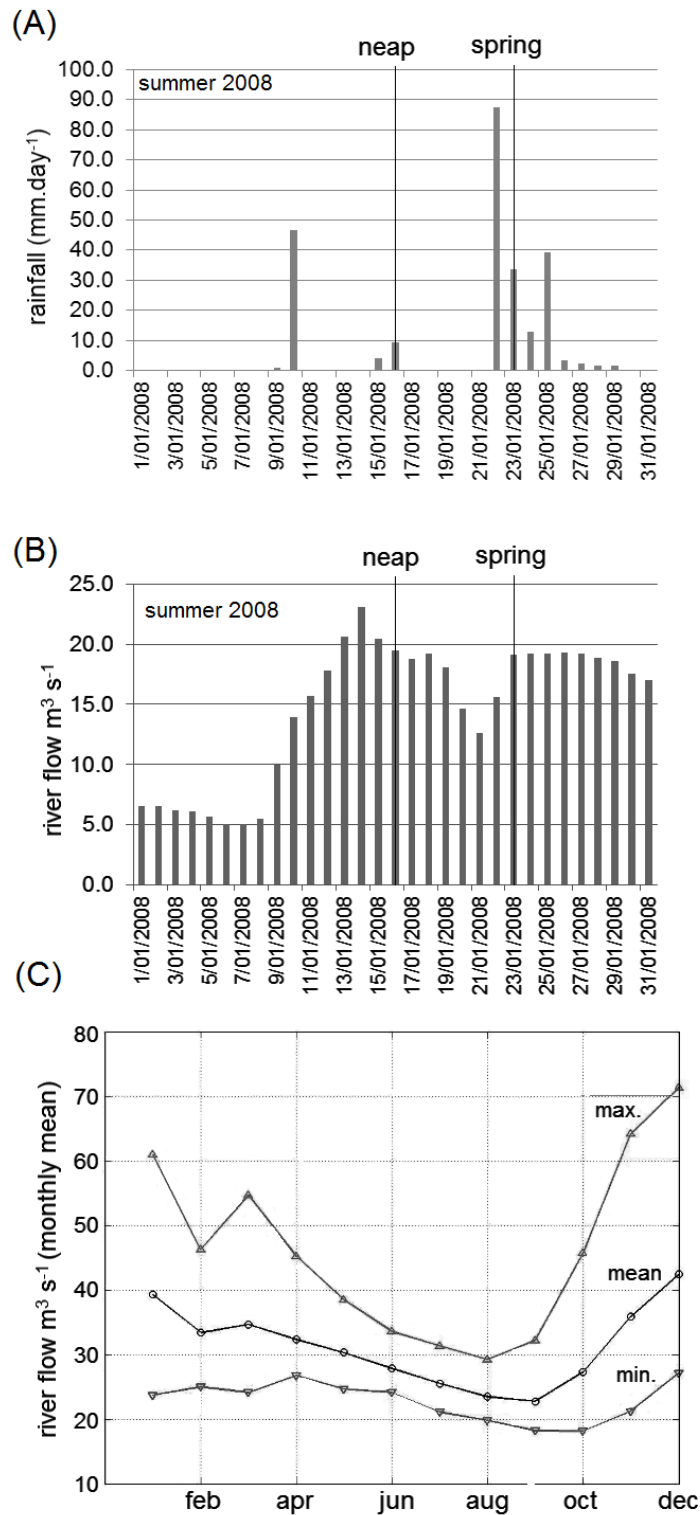


Figure 3 – Daily variation of the rainfall (A), and river discharge (B) during January (2008), observations were made at the gauge station *Helvécia* n° 55510000 (código 1739006) – National Agency of Waters. (C) Climatological estimate of the mean, minimum (min.) and maximum (max.) monthly river discharge using data from 1975 to 2008 (34 years of measured river flow) and corrected using the factor 1.6 to account for the entire drainage basin area of the *Peruípe* River.

Figure 4

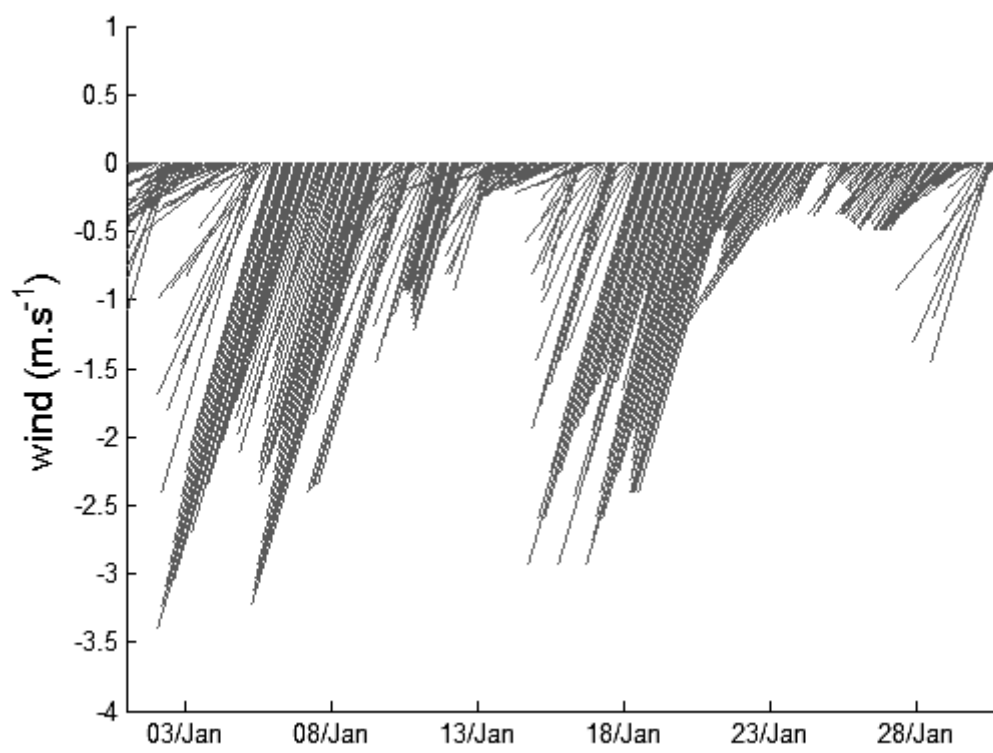


Figure 4 – Wind data obtained from the Instituto Nacional de Meteorologia INMET. Data during January 2008 at Caravelas station, code INMET A405, and coordinates (Lat. 17°43'48.0" S; Long. 39°15'00.0" W).

Figure 5

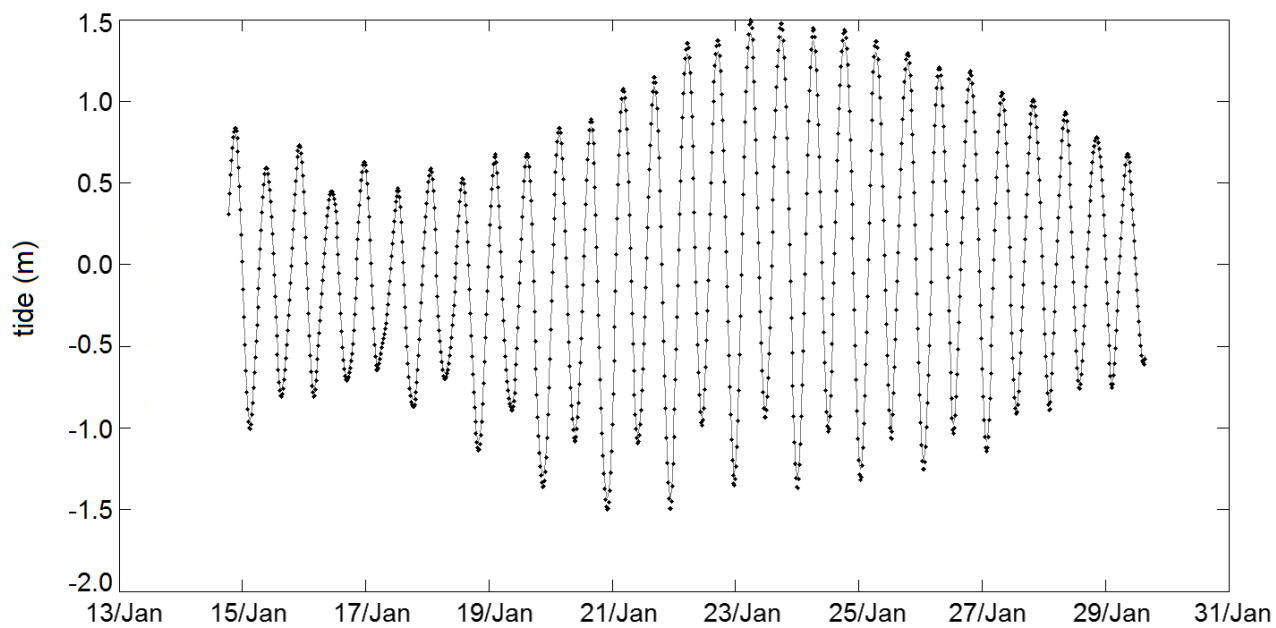


Figure 5 – Modelled water column (m) at station A compared to measured tides, from 14th to 29th of January 2008. Dots denote observations, and line denotes model result.

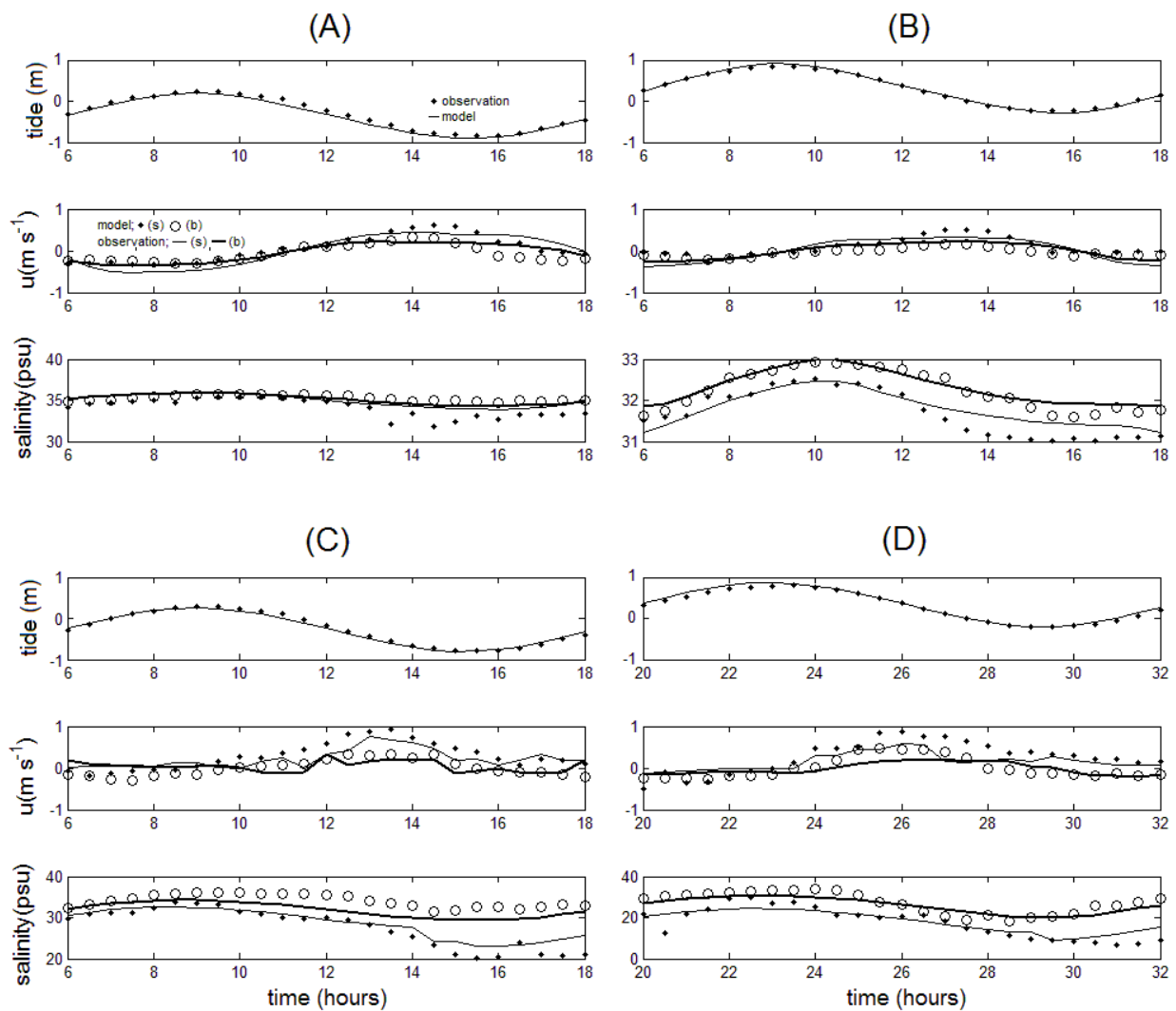


Figure 6 – Modelled tide (m), axial channel velocity u (m s^{-1}) and salinity (psu) compared to measured time series at stations A, B, C, and D, during neap tides. Measurements and simulation represented at the surface and bottom layers. Skill values are synthesised in Table 4.

Figure 7

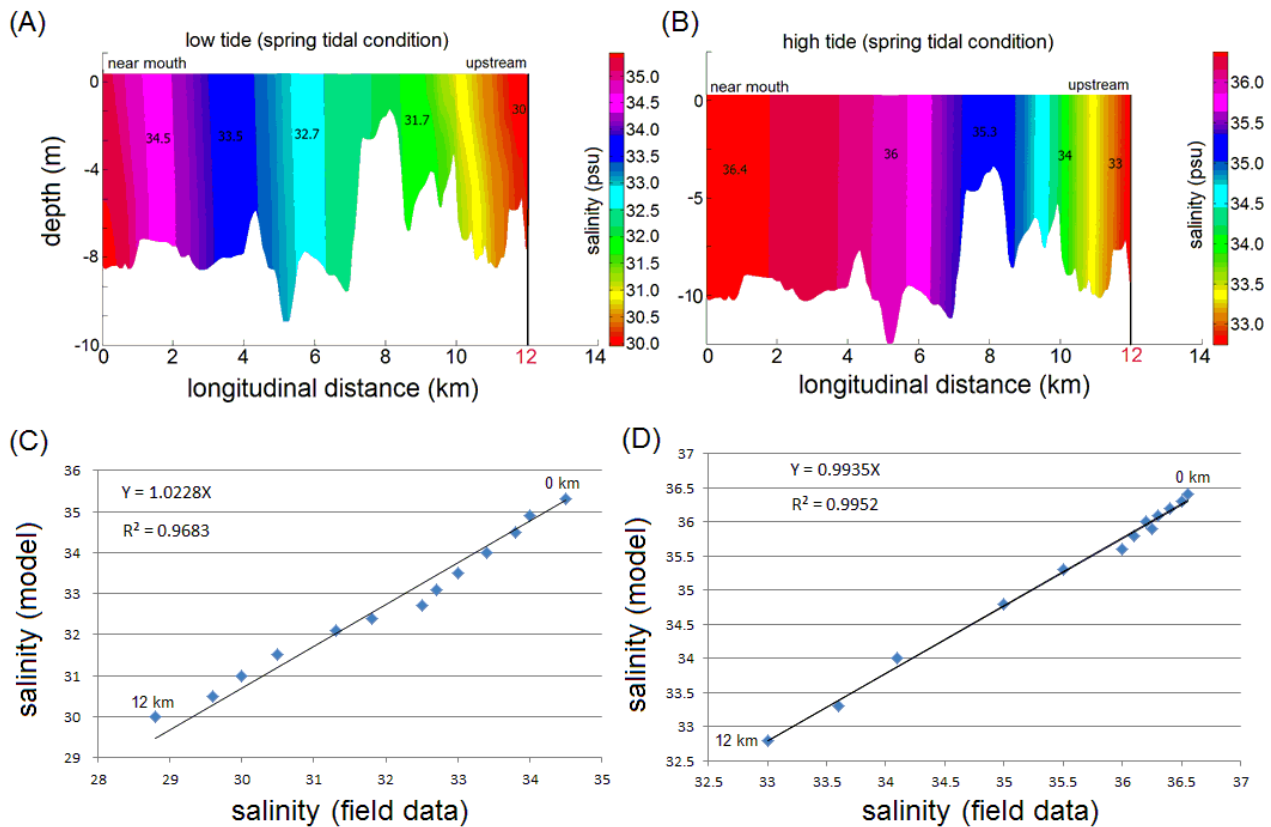


Figure 7 – Axial distribution of salinity () in the Caravelas Estuary in spring tidal conditions, at low (A) and high (B) tide. Correlation of axial distribution of the mean water column salinity between model and observation at low (C) and high (D) tide in spring tide, where Y and X denote model results and measurement, respectively. First dot on left denotes position at estuarine mouth (0 km), while last dot denotes a position 12 km further upstream, the increment of 1 km is applied from first to last dot. Observations obtained from Schettini and Miranda (2010).

Figure 8

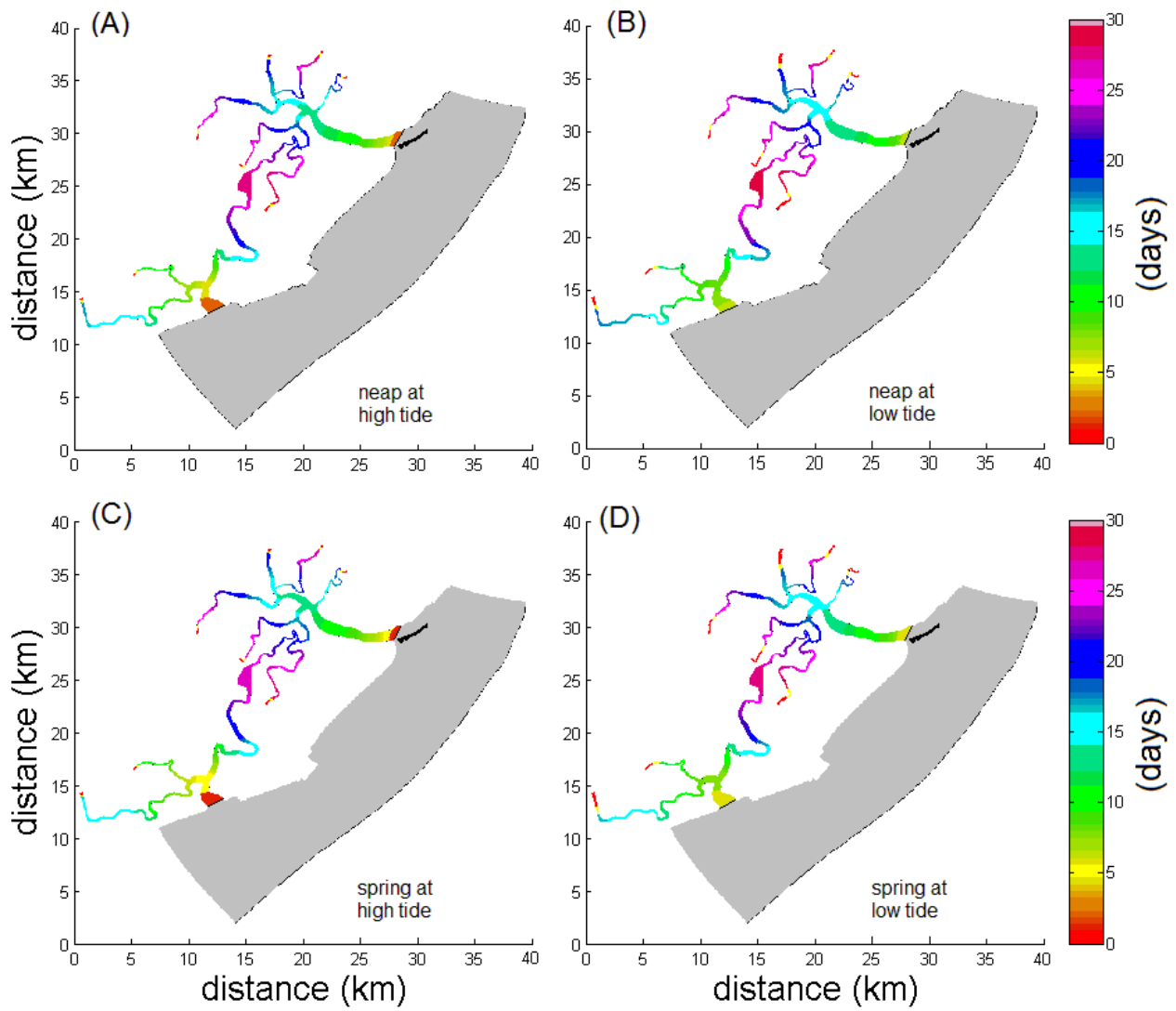


Figure 8 – Verically averaged residence time spatial distribution (φ), for scenarios S_1 (A), S_2 (B), S_3 (B) and S_4 (C). Colored bar indicates the timescales in days.

Figure 9

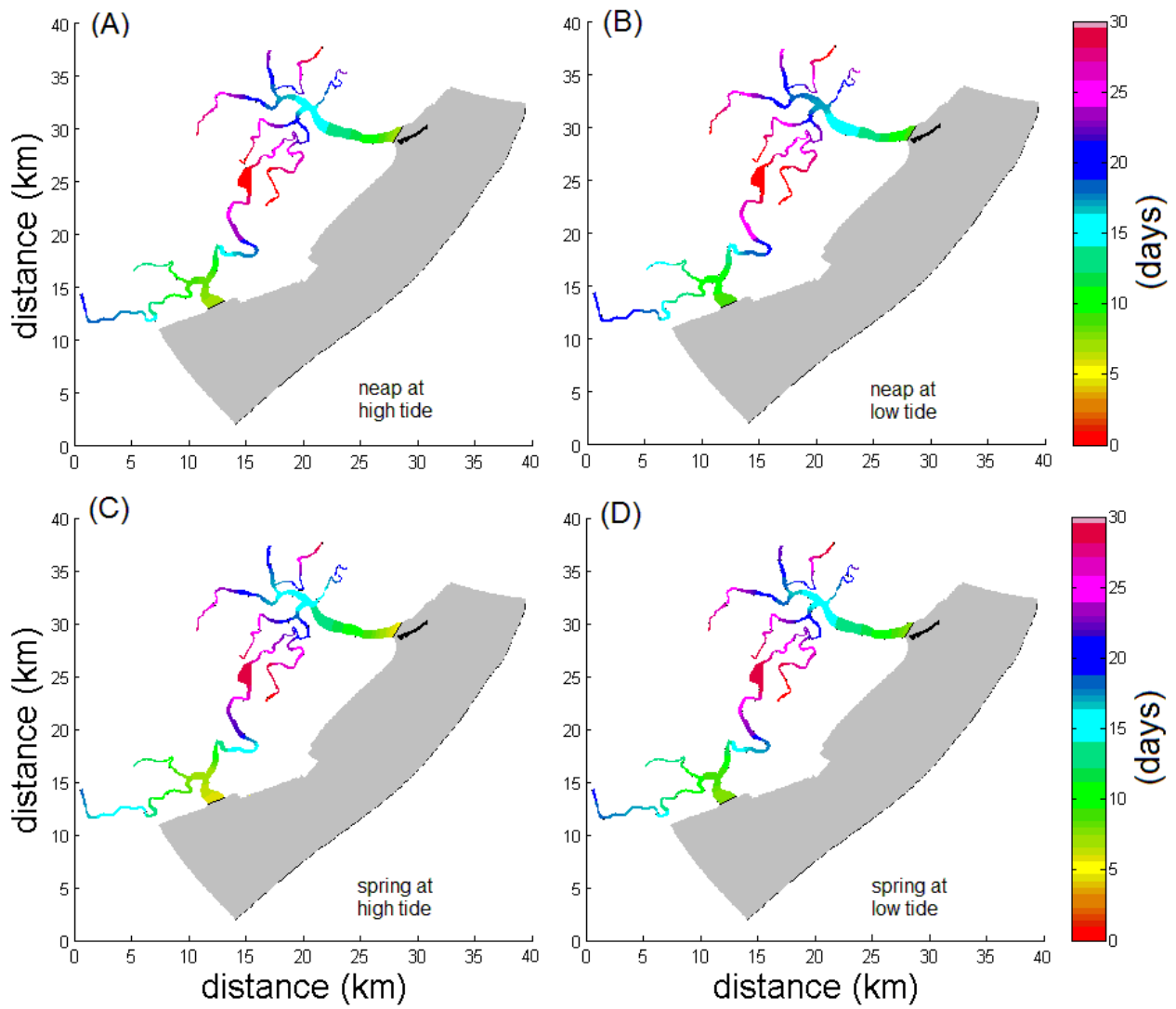


Figure 9 – Vertically averaged exposure time spatial distribution (Θ), for scenarios S_1 (A), S_2 (B), S_3 (B) and S_4 (C). Colored bar indicates the timescales in days.

Figure 10

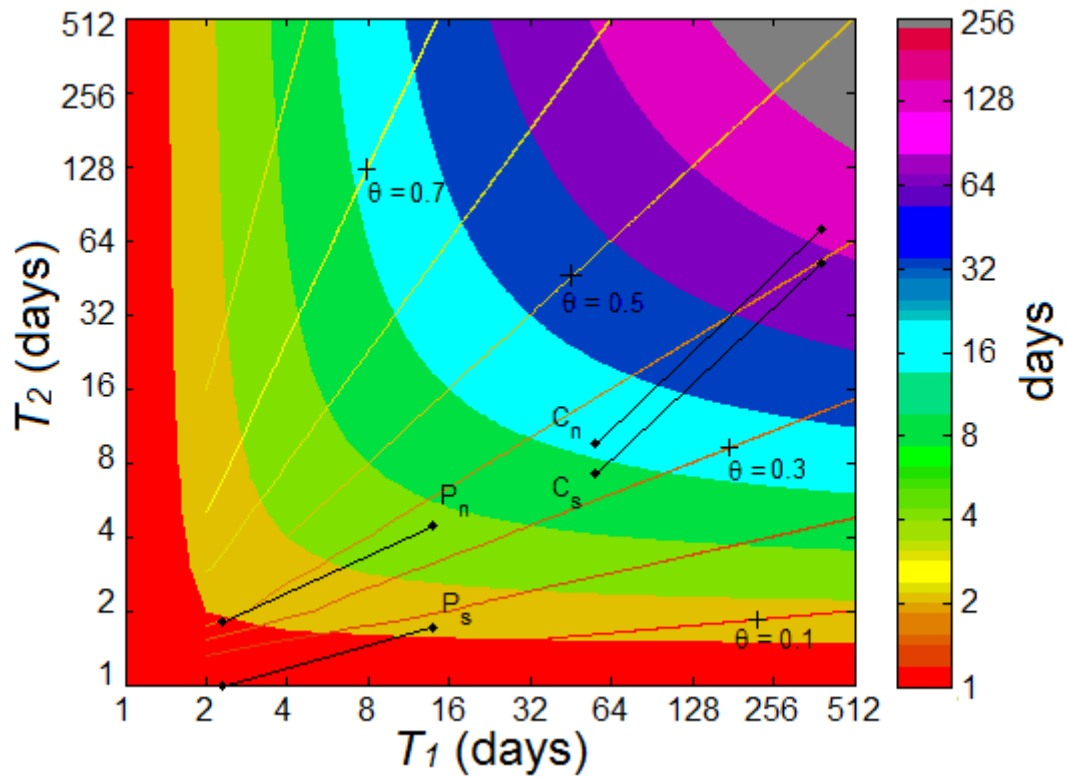


Figure 10 – The position of Caravelas (CA) and Peruípe (P) estuaries on the advection-diffusion diagram to indicate the relative contribution to the water renewal T_P by the advective (T_1) and dispersive (T_2) timescales using a logarithmic scale. Subscript (n) and (s) indicate neap and spring tide conditions.

Figure 11

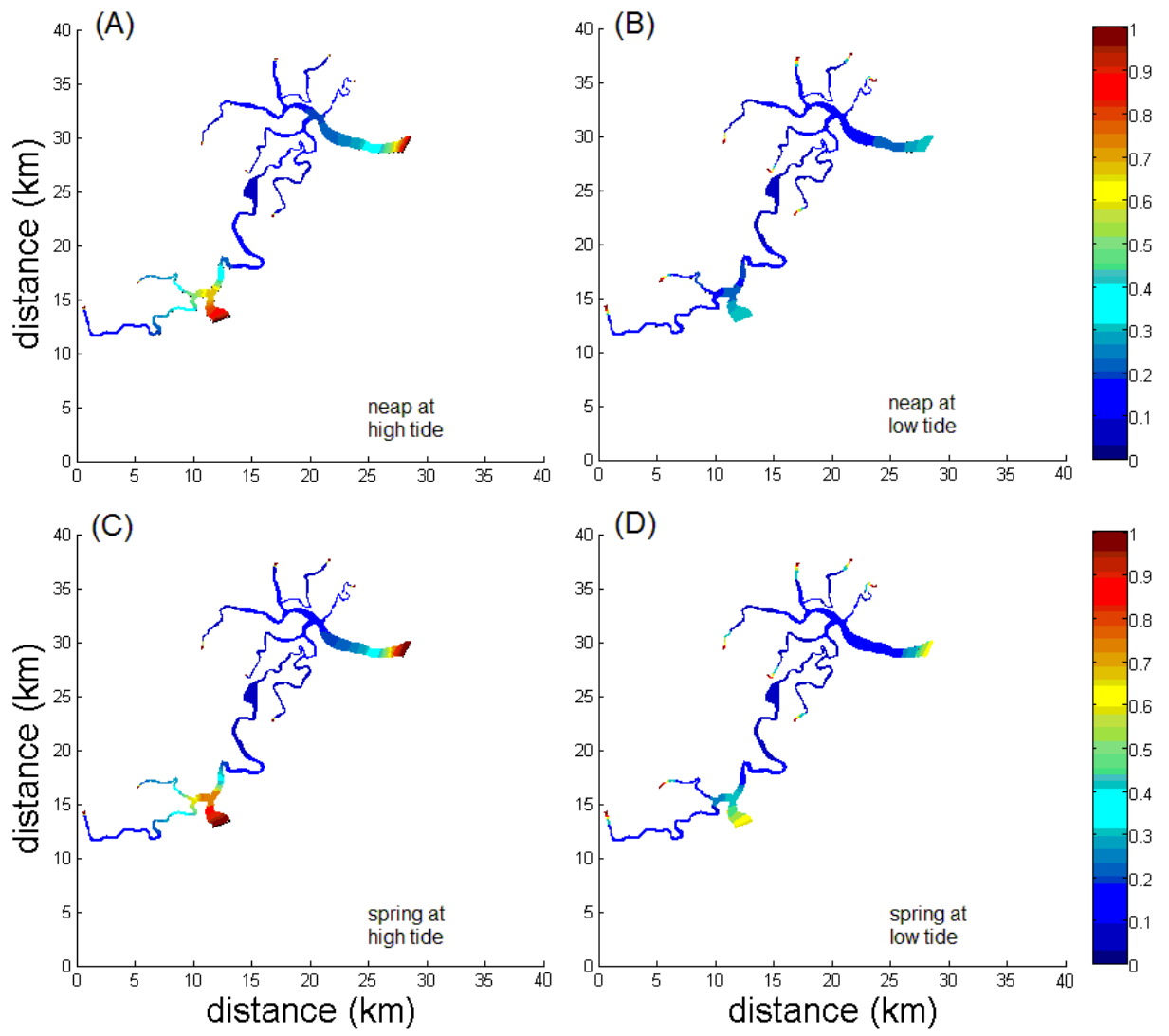


Figure 11 – Return coefficient spatial distribution (r), for scenarios S_1 (A), S_2 (B), S_3 (B) and S_4 (C). Colored bar indicates the timescales in days.

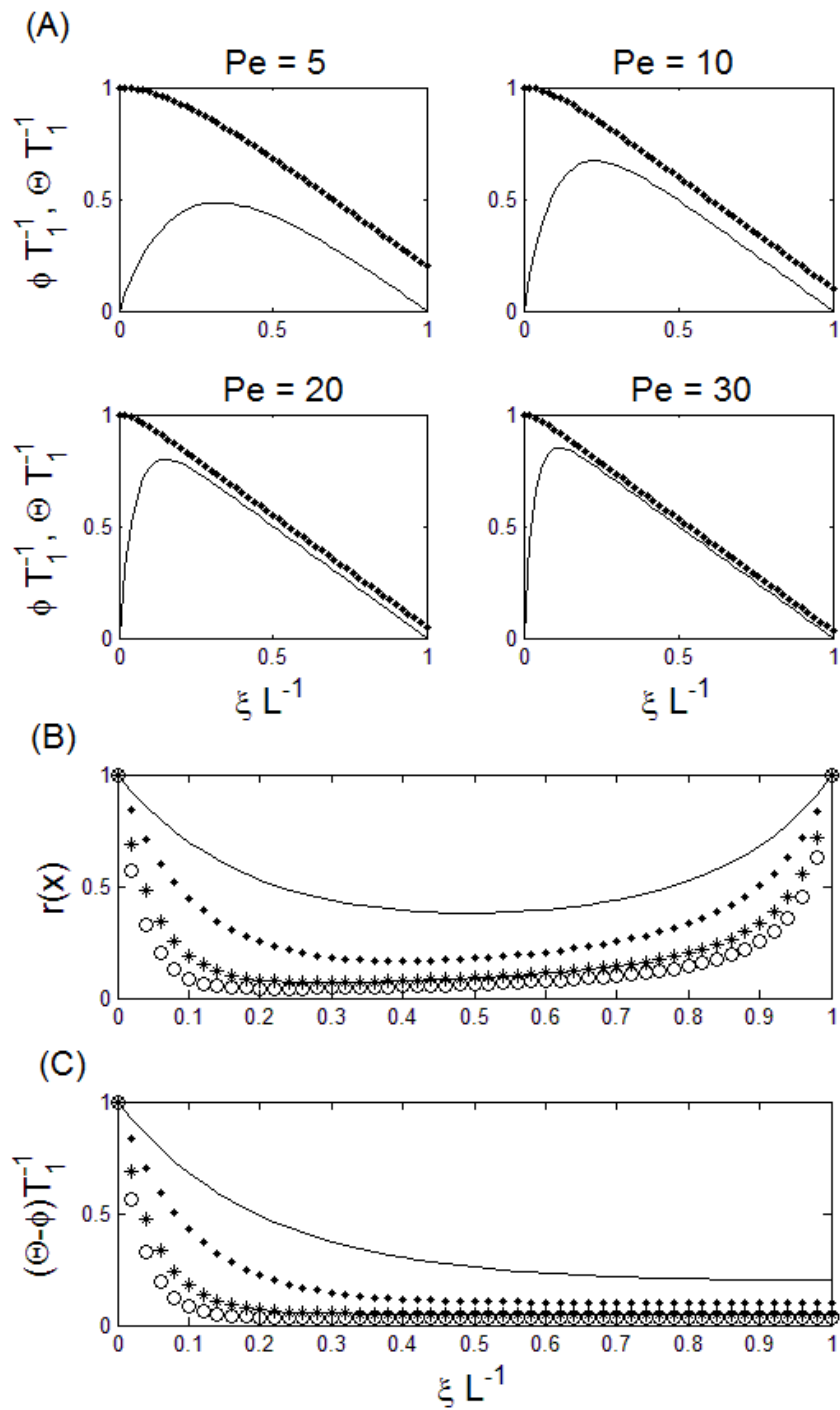


Figure 12 – (A) Representation of the exposure time Θ (dots) and residence time ϕ (line) as a function of the distance x from the upstream boundary of the domain. (B) Return coefficient and (C) and the difference between the exposure and residence time $(\Theta - \phi)$ calculated for different values of Peclet number, $Pe = 5$ (line), $Pe = 10$ (dot), $Pe = 20$ (star), and $Pe = 30$ (circle). The timescales are normalised by means of the advective timescale T_1 .

Table 1 – Summary of flow conditions in the simulations for the Peruípe, Cupído, and Jaburuna rivers. Data from ANA.

river	flow ($\text{m}^3 \text{s}^{-1}$)	typical range of flow ($\text{m}^3 \text{s}^{-1}$)	Salinity applied to
	January 2008	in wet season	boundary cells
Peruípe	~5-20	17 to 70	0
Cupído	2	2 to 9	6
Jaburuna	2		4

Table 2 – Amplitude and frequency of the main tidal components recorded at Terminal Aracruz - TA.

Component	Amplitude (cm)	Frequency (degree hr ⁻¹)
O ₁	8.89	13.94
K ₁	5.76	15.04
P ₁	1.91	14.96
Q ₁	1.62	13.40
M ₂	75.10	28.98
S ₂	33.48	30.00
L ₂	15.06	29.53
N ₂	13.45	28.44
K ₂	9.11	30.08

Table 3 – Sensitivity analysis of the salinity to the value of the horizontal diffusivity K_h using the Skill method from Wilmott (1981). Skill values are in the range 0 to 1. The factor f was used in the sensitivity analyses following formulae by Okubo (1971).

Parameter	Site A (Skill)	Site B (Skill)	Site C (Skill)	Site D (Skill)
$f = 2$				
Salinity (neap)	0.78	0.58	0.55	0.70
Salinity (spring)	0.85	0.62	0.60	0.75
$f = 100$				
Salinity (neap)	0.86	0.72	0.68	0.74
Salinity (spring)	0.90	0.76	0.75	0.82
$f = 150$				
Salinity (neap)	0.80	0.76	0.64	0.72
Salinity (spring)	0.95	0.80	0.80	0.88
$f = 200$				
Salinity (neap)	0.85	0.80	0.73	0.78
Salinity (spring)	0.97	0.85	0.83	0.93
$f = 250$				
Salinity (neap)	0.81	0.77	0.72	0.74
Salinity (spring)	0.94	0.81	0.78	0.89
$f = 400$				
Salinity (neap)	0.81	0.74	0.66	0.65
Salinity (spring)	0.85	0.78	0.70	0.79
$f = 2000$				
Salinity (neap)	0.64	0.56	0.50	0.60
Salinity (spring)	0.66	0.60	0.54	0.65

Table 4 – Results of the validation using the Skill method from Wilmott (1981).

Parameter	Site A (Skill)	Site B (Skill)	Site C (Skill)	Site D (Skill)
Tidal height (neap)	0.99	1	0.99	0.99
Tidal height (spring)	1	0.99	1	0.98
Velocity (neap)	0.68	0.65	0.62	0.65
Velocity (spring)	0.77	0.93	0.84	0.88
Salinity (neap)	0.85	0.80	0.73	0.78
Salinity (spring)	0.97	0.85	0.83	0.93
Parameter	Site A (Skill)	Site B (Skill)		
Velocity (14 th to 26 th Jan 2008)	0.72	0.78		

Appendix 1

[Click here to download Supplementary material for on-line publication only: Andutta-et.al-2015-Caravelas-Appendix 01.doc](#)

